Journal of Neuroinflammation

RESEARCH

Open Access

The regulation of NFKB1 on CD200R1 expression and their potential roles in Parkinson's disease

Suzhen Lin[1†], Yimei Shu[1†], Ruinan Shen[1†], Yifan Zhou[1], Hong Pan[1], Lu He[1], Fang Fang[3], Xue Zhu[1], Xinrui Wang[4], Ying Wang[1], Wei Xu[1] and Jianqing Ding[2*]

Abstract

Background Overactivated microglia are a key contributor to Parkinson's disease (PD) by inducing neuroinflammation. CD200R1, a membrane glycoprotein mainly found on microglia, is crucial for maintaining quiescence with its dysregulation linked to microglia's abnormal activation. We and other groups have reported a decline in CD200R1 levels in several neurological disorders including PD. However, the mechanism regulating CD200R1 expression and the specific reasons for its reduction in PD remain largely unexplored. Given the pivotal role of transcription factors in gene expression, this study aimed to elucidate the transcriptional regulation of CD200R1 and its implications in PD.

Methods The CD200R1 promoter core region was identified via luciferase assays. Potential transcription factors were predicted using the UCSC ChIP-seq database and JASPAR. NFKB1 binding to the CD200R1 core promoter was substantiated through electrophoretic mobility shift and chromatin immunoprecipitation assays. Knocking-down or overexpressing NFKB1 validated its regulatory effect on CD200R1. Correlation between decreased CD200R1 and deficient NFKB1 was studied using Genotype-Tissue Expression database. The clinical samples of the peripheral blood mononuclear cells were acquired from 44 PD patients (mean age 64.13 ± 9.78, 43.2% male, median Hoehn-Yahr stage 1.77) and 45 controls (mean age 64.70 ± 9.41, 52.1% male). NFKB1 knockout mice were utilized to study the impact of NFKB1 on CD200R1 expression and to assess their roles in PD pathophysiology.

Results The study identified the CD200R1 core promoter region, located 482 to 146 bp upstream of its translation initiation site, was directly regulated by NFKB1. Significant correlation between NFKB1 and CD200R1 expression was observed in human PMBCs. Both NFKB1 and CD200R1 were significantly decreased in PD patient samples. Furthermore, NFKB1-/- mice exhibited exacerbated microglia activation and dopaminergic neuron loss after 1-methyl-4-phenyl-1,2,3,6-tetrahydropyridine (MPTP) treatment.

†Suzhen Lin, Yimei Shu and Ruinan Shen contributed equally to this work.

*Correspondence:
Jianqing Ding
jqding18@shsmu.edu.cn

Full list of author information is available at the end of the article

Conclusion Our study identified that NFKB1 served as a direct regulator of CD200R1. Reduced NFKB1 played a critical role in CD200R1 dysregulation and subsequent microglia overactivation in PD. These findings provide evidence that targeting the NFKB1-CD200R1 axis would be a novel therapeutic strategy for PD.

Keywords Parkinson's disease, CD200R1, NFKB1, Microglia, Promoter, Transcription factor

Introduction

Parkinson's disease (PD) ranks the second most prevalent neurodegenerative disorder worldwide, characterized by dopaminergic neuron loss and alpha-synuclein (α-syn) aggregation in the substantia nigra (SN) [1]. Neuroinflammation plays a pivotal role in PD's pathophysiology, with elevated inflammation markers observed in the brain, serum, and cerebrospinal fluid from PD patients, correlating with disease severity and disability [2–5].

Microglia are the principal innate immune cells in the central nervous system (CNS) and densely populated in the SN. Histopathological studies have long shown activated microglia in PD patients' brains [6]. Recently, imaging studies provided in vivo evidence of early microglial activation in the disease process [7]. Activated microglia produce pro-inflammatory factors such as tumor necrosis factor (TNF), interleukin (IL)-1β, contributing to neurotoxicity and neurodegeneration [8]. Preclinical studies suggest that suppressing these detrimental pro-inflammatory functions can be neuroprotective in PD models [9].

In the non-diseased CNS, microglia exhibit the homeostasis phenotype expressing inhibitory molecules like CX3CR1, TGF-receptor 1 (TGFBR1) and CD200R1 [10]. CD200R1, an Ig superfamily transmembrane glycoprotein, is expressed chiefly by myeloid cells and microglia. Its ligand, CD200, is mainly expressed by neurons in the CNS and is also seen in astrocytes and oligodendrocytes especially in pathological conditions. First investigated in the experimental model of multiple sclerosis [11], it has been well established that CD200R1-CD200 interaction mainly results in the inhibition of pro-inflammatory microglial activation. Enhanced proliferation of activated microglia and boosted pro-inflammatory mediators are observed in CD200 deficient models or CD200R1-blocking conditions while upregulated CD200 expression or activation of CD200R1 with CD200Fc, a CD200R agonist could suppress the inflammation [12].

Alterations in CD200-CD200R1 system have been reported in both experimental PD models and PD patients. Our previous work demonstrated downregulated of CD200 and CD200R1 in the brain of 1-Methyl-4-phenyl-1,2,3,6-tetrahydropyridine (MPTP)-induced PD mice with simultaneous increase of pro-inflammatory mediators, accompanied by enhanced microglia activation and loss of nigrostriatal dopaminergic neurons [13]. These biochemical and histological changes could be exacerbated by blocking CD200R1 in rats with peripheral lipopolysaccharide (LPS) treatment [14] and our group got similar findings in 6- hydroxydopamine (OHDA) -injected rats [15]. We also observed that blockade of CD200R selectively and significantly enhanced dopaminergic neurons' susceptibility to neurotoxicity triggered by rotenone and iron in mesencephalic neuron/glia cultures [16]. Likewise, microglia activation was aggravated after MPTP administration in CD200 knockout mice compared to their wildtype counterparts [17] and correspondingly, supplementing CD200/CD200Fc remarkably depressed the release of inflammatory factors from microglia induced by MPTP, LPS or α-syn [13, 18], as well as attenuating dopaminergic neuronal death [17]. Interestingly, work conducted by Wang's group also showed that compared to CX3CR1, CD200R1 was more sensitively inhibited in microglia after LPS or α-syn challenge, indicating a more important involvement of CD200R1 in PD pathogenesis [18]. Clinical evidence from our group showed that peripheral blood mononuclear cells (PBMCs) from PD patients could not effectively upregulate CD200R1 in response to inflammatory stimulations [19]. These findings indicate that targeting CD200R1 dysregulation may represent a viable therapeutic strategy for mitigating microglial activation and neurodegeneration in PD.

The mechanism of downregulated CD200R1 expression in PD remains unclear. Transcription factor-promoter combination is fundamental for gene expression regulation. Two transcription factors of CD200R1, CAAT/enhancer-binding protein-β (C/EBPβ) [20] and proliferator-activated receptor gamma (PPARγ [21] have been reported. However, CD200R1 mRNA basal levels in microglia was not modified by either of these two transcription factors [20, 21]. In addition, these findings were based on the predicted promoter sequence of murine CD200R1 while research in mankind is yet absent.

In this study, we aimed to identify the transcription factors decisively responsible for regulating human CD200R1. For this purpose, we would first figure out its core promoter. Our previous work defined the promoter region of human CD200R1 with approximately 700 bp [22], but a more precise definition is still needed in order to confidently discover the critical regulatory elements in this system. Furthermore, we sought to evaluate the impact of these transcriptional regulators on microglia activation and dopaminergic neuron loss, combined with their relevance to PD pathophysiology.

Materials and methods

Cell culture and treatment

HEK293T was cultured in Dulbecco's modified Eagle's medium (DMEM, Gibco) supplemented with 10% fetal bovine serum (FBS, Gibco), 100 U/ml penicillin, and 100 ug/ml streptomycin (Gibco); and incubated at 37 °C with 5% carbon dioxide (CO2). The human monocyte cell line U937 was maintained in Roswell Park Memorial Institute 1640 Medium (RPMI 1640 Medium) medium (Nacalai Tesque, Kyoto, Japan) containing 10% FBS, along with 100 U/ml penicillin, 100 U/ml streptomycin, and 10 mg/mL neomycin, under incubation conditions of 37 °C and 5% CO2. The microglial cell line BV2 cells were cultured in high-glucose DMEM supplemented with 5% FBS and maintained in a 5% CO2 incubator.

Primary microglia were cultured from postnatal day 1 C57BL/6 mice, with brains mechanically dissociated, devoid of meninges and vasculature, and filtered through a 70-um nylon mesh. Tissues were further incubated with 0.25% trypsin (15090046, Gibco) and 1 mg/ml DNase I (10104159001, Roche). The cell suspension was centrifuged for 4 min at 800 rpm using a tabletop microfuge at 37 °C. The pellet was then resuspended in the culture medium. Isolated cells were cultured for 14 days in DMEM/F12 (Gibco) supplemented with 10% FBS. After 10–14 days, when a mixed glia culture is established, flasks were incubated with trypsin solution (0.25% trypsin and 1 mM EDTA in Hank's balanced salt solution) in DMEM/F12 with a 1:4 dilution, followed by subjected to mild shaking (200 rpm for 2 h) to detach microglia from the astrocyte layer. The supernatant was collected and centrifuged, with the pellet being microglia which were cultured with DMEM/F12 containing 10% FBS. Subsequent experiment was carried out when the primary microglia reached 95% purity.

Detailed information regarding experimental procedures conducted on these specific cell lines can be found in the corresponding sections of the Methods section. Briefly, HEK293T, U937, and BV2 cell lines were transfected with the plasmids of candidate transcription factors in combination with CD200R1 promoter plasmid to elucidate their regulatory roles on CD200R1 promoter activity by luciferase reporter assays (refer to the 'Luciferase Reporter Assays' section for detailed protocols). Additionally, HEK293T cells were employed in Electrophoretic mobility shift assay (EMSA) where cells were transfected with NFKB1 expression vectors or control constructs (further details are available in the 'EMSA' section). Furthermore, HEK293T cells were transfected with NFKB1-siRNA or a negative control to explore the effects of decreased NFKB1 on CD200R1 expression levels (further details are available in the 'siRNA and Transfection' section). Primary microglia isolated from mice with genotypes NFKB1+/+, NFKB1+/-, and NFKB1-/- were utilized to measure basal CD200R1 mRNA in these mice (for methodological details, refer to the 'Quantitative RT-PCR (qRT-PCR)' section).

Isolation and culturing of peripheral blood mononuclear cells (PBMCs)

The sample collection protocol was approved by the Health Research Ethic Authority of Ruijin Hospital Affiliated to Shanghai Jiaotong University School of Medicine and the written informed consent was obtained from each donor. The isolation method for PBMCs is well-established and validated in our previous work [23]. About 5 ml of blood was collected using BD Vacutainer tubes containing acid-citrate-dextrose anticoagulant. The PBMCs were isolated using Ficoll-Paque gradient centrifugation (MilliporeSigma, USA). The centrifugation was carried out at a speed of 2000 rpm for 20 min at room temperature. The PBMCs were then seeded at a density of 4×104 cells per well in 96-well plates for cell-based enzyme-linked immunosorbent assay (ELISA) assay and 2×105 cells per well in 24-well plates for mRNA analysis. The cells were cultured in RPMI 1640 Medium (Life Technologies) supplemented with 10% FBS under 37 °C with 5% CO2. Cell viability was assessed with the trypan blue staining.

Gene Silencing with siRNA

We employ siRNA technology to selectively knockdown NFKB1 to elucidate the regulatory influence of NFKB1 on CD200R1 expression in PD. We designed the siRNA sequence targeting the human NFKB1 gene, as presented in Table 1. The negative control siRNA were obtained from RiboBio (Guangzhou, China) and the catalog number is siN0000001-1-10.

Through a series of optimization experiments, optimal conditions for siRNA transfection in HEK293T cells were identified as follows. The ideal seeding density was determined to be 2×105 cells per well in a 6-well plate. Maximum transfection efficiency was achieved with a 1:1 ratio of siRNA to transfection reagent and a final siRNA concentration of 12.5 pmol/ml. Cells were transfected for 48 h to reach the most effective gene silencing.

For PBMCs, various experiments were conducted to refine the conditions based on the intended applications. For cell-based enzyme-linked immunosorbent assay (ELISA), PBMCs were seeded at a density of 4×104 cells per well in 96-well plates, with an siRNA concentration of 9 pmol/ml. For Quantitative RT-PCR, the preferred seeding density was 2×105 cells per well in 24-well plates, with an siRNA concentration of 16 pmol/ml per well. In both cases, the transfection efficiency was maximized by using a 1:1 ratio of siRNA to transfection reagent and a transfection period of 48 h.

Table 1 Primer Sequences[a]

Name of the primer	Sequence 5′ to 3′	Note
CD200R1p-1989 Forward	TGCACAACAGAGACTTAACCC	Forward primer
CD200R1p-1519 Forward	TCCATGCCCTCAAGGATCTG	Forward primer
CD200R1p-1100 Forward	AAAGGTGAAACTGAATGGCAATAA	Forward primer
CD200R1p-876 Forward	AGGGTCACAGTCAGAGAAGATGTG	Forward primer
CD200R1p-704 Forward	CCATTTCAGACTTCTGATCACC	Forward primer
CD200R1p-583 Forward	AGGGTTGTGTGTTGACTCCC	Forward primer
CD200R1p-482 Forward	TCAACCTGGAGAAAGCCTCT	Forward primer
CD200R1p-315 Forward	GAGAGGAGAACCAATGAGCT	Forward primer
CD200R1p-266 Forward	CGTCTTTGCTTCAGGGCTTC	Forward primer
CD200R1 Reverse	CTAGCCCCTTCCTTCACGTC	Reverse primer
CD200R1p Deletion-482 to -267 Forward	TACTAAGGCCGTAAAGCTCTCGTCTTTGCTTCAGGGCTTC	Forward primer for deletion construct
CD200R1p Deletion-482 to -267 Reverse	GAAGCCCTGAAGCAAAGACGAGAGCTTTACGGCCTTAGTA	Reverse primer for deletion construct
CD200R1 CHIP qPCR Forward	TACAGGAAATCTATTGCTGT	qPCR primer for CHIP assay
CD200R1 CHIP qPCR Reverse	CTAGCCCCTTCCTTCACGTC	qPCR primer for CHIP assay
CD200R1 mRNA qPCR Forward	TGCTGTGTCAAGTTCCAGAG	qPCR primer for mRNA
CD200R1 mRNA qPCR Reverse	CTTCCTTCTAGCCCCTTCCT	qPCR primer for mRNA
Cd200r1 mRNA qPCR Forward[b]	TACGAGTGAATCACACAGCA	qPCR primer for mRNA (mouse)
Cd200r1 mRNA qPCR Reverse[b]	CAGGACACATCAGACACATTG	qPCR primer for mRNA (mouse)
NFKB1 mRNA qPCR Forward[b]	GGACCAGCAAAGGTTATTGTT	qPCR primer for mRNA
NFKB1 mRNA qPCR Reverse[b]	AGATCCCATCCTCACAGTGTT	qPCR primer for mRNA
Nfkb1 mRNA qPCR Forward[b]	AGAGGATTTGCTGAGGGTTG	qPCR primer for mRNA (mouse)
Nfkb1 mRNA qPCR Reverse[b]	TGCTGAGGATTCTGTCGTGT	qPCR primer for mRNA (mouse)
siRNA for NFKB1	GATCCTTCTTTGACTCATA	siRNA sequence

[a] The numbers after the symbol "-" indicate the distance from the CD200R1 translation start site; The siRNA sequence is listed without a 5′ to 3′ notation as it is a small interfering RNA and not a primer; qPCR refers to quantitative polymerase chain reaction

[b] The sizes of relevant qPCR products are as follows: 92 base pairs (bp) for human CD200R1, 84 bp for mouse Cd200r1, 97 bp for human NFKB1, and 104 bp for mouse Nfkb1

Table 2 Plasmid list[a]

Plasmid Name	Forward Primer Position		Reverse Primer Position		Length (bp)	Description
	Start Position	End Position	Start Position	End Position		
CD200R1p-1989 ~-146	-1989	-1969	-166	-146	1844	Full-length promoter fragment
CD200R1p-1519 ~-146	-1519	-1499	-166	-146	1374	Promoter fragment
CD200R1p-1100 ~-146	-1100	-1080	-166	-146	955	Promoter fragment
CD200R1p-876 ~-146	-876	-856	-166	-146	731	Promoter fragment
CD200R1p-704 ~-146	-704	-684	-166	-146	559	Promoter fragment
CD200R1p-583 ~-146	-583	-563	-166	-146	438	Promoter fragment
CD200R1p-482 ~-146	-482	-462	-166	-146	337	Promoter fragment
CD200R1p-365 ~-146	-365	-345	-166	-146	220	Promoter fragment
CD200R1p-266 ~-146	-266	-246	-166	-146	121	Promoter fragment
CD200R1p-deletion-482 ~-267	-1989	-1969	-166	-146	1628	Promoter fragment constructed by deleting the −482 to −267 bp region from the larger −1989 to −146 bp segment

[a] The numbers after the symbol "-" indicate the distance from the CD200R1 translation start site; The "Length (bp)" column indicates the length of the promoter fragment in base pairs. The "Description" column provides additional details about the plasmid, such as whether it contains a deletion mutation

Construction of luciferase reporter gene vectors and luciferase reporter assays

The luciferase reporter plasmids were constructed following these steps. First, CD200R1 promoter sequences were amplified from HEK293T genomic DNA using PCR. The primers used for amplification can be found in Table 1. The positions of the primers and the lengths of the products are listed in Table 2. A touchdown PCR was employed using a high-fidelity DNA polymerase (Takara, R045A, Dalian, China). This procedure consisted of an initial denaturation step at 94℃ for 3 min, followed by 10 cycles of denaturation at 98℃ for 15 s, annealing from 68℃ to 53℃ with a decrease of 1.5℃ per cycle, and extension at 72℃ for 60 s per cycle. This was followed by

20 cycles of denaturation at 98℃ for 15 s, annealing at 55℃ for 15 s, and extension at 72℃ for 60 s per cycle. Finally, an additional extension was performed at 72℃ for 5 min. The PCR products were then purified and cloned into pGL3-basic luciferase plasmids (Promega, Beijing, China).

For the generation of the plasmic containing the −1989 to -146 bp promoter fragment with deletion of -482 to -267 bp region, specific primers (CD200R1p Deletion-482 to -267 Forward/Reverse) were designed. One fragment was amplified using "CD200R1p-1989 Forward" as the forward primer and "CD200R1p Deletion-482 to -267 Reverse" as the reverse primer while the other fragment was produced with "CD200R1p Deletion-482 to -267 Forward" as the forward primer and "CD200R1 Reverse" as the reverse primer. CD200R1p Deletion-482 to -267 Reverse" is the reverse primer with the sequence of -502 bp to -483 bp with a 20 bp homologous arm sequence at the 5' end ranging from −266 bp to -247 bp. Similarly, "CD200R1p Deletion-482 to -267 Forward" is the forward primer with the sequence of -266 bp to -247 bp with a 20 bp homologous arm sequence at the 5' end ranging from −502 bp to -483 bp. The clones were subjected to sequencing analysis to confirm the accuracy of the sequence.

For the luciferase assay, the Firefly luciferase reporter plasmids, which contain various truncated fragments of the CD200R1 promoter, were co-transfected with the Renilla luciferase control plasmid PRL-SV40. The ratio of Firefly to Renilla plasmids used was 49:1. An empty pGL3-basic plasmid was used as the negative control. The expression level of the Firefly luciferase is directly proportional to the promoter activity of the CD200R1 fragments, while the Renilla signal serves as an internal control for variations in transfection efficiency. The transcriptional activity was measured using the Dual-Luciferase Reporter Assay System (Promega, E1980) on a Synergy™ H4 Hybrid Microplate Reader (Biotek, Shanghai, China). Each sample was read in duplicate, and the results were reported as the ratio of Firefly to Renilla luciferase activity.

Quantitative RT-PCR (qRT-PCR)

Total RNA was extracted from approximately 1.5×105 human PBMCs (initially seeded at a concentration of 2×105 cells per well in 24-well plates) or about 5×105 mouse primary microglia using the HiPure RNA Mini kit (Magen, Shanghai, China). The quality and concentration of the RNA were confirmed using a Synergy™ H4 Hybrid Microplate Reader (Biotek, Shanghai, China), an A260/280 ratio between 1.9 and 2.1 indicating high purity.

Reverse transcription was performed using the PrimeScript RT reagent kit with gDNA Eraser (Takara) in a 20 μL reaction volume, using 1 μg total RNA, following the manufacturer's protocol with an incubation at 50 °C for 15 min, followed by 85 °C for 5 s to inactivate the enzyme.

For qRT-PCR, the reaction mixture was consisted of 10 μL SYBR Premix Ex Taq II (Takara, RR420), 5 μL of 10-fold diluted cDNA from the above reverse transcription, 0.2 μM of each primer, and nuclease-free water to a final volume of 20 μL. The 7500 Real-Time PCR System (Applied Biosystems, USA) was used with the following setting: initial denaturation at 95℃ for 30 s, followed by 40 cycles of denaturation at 95℃ for 5 s and annealing / extension at 60℃ for 34 s. The stability of expression of the endogenous reference genes (SRPS6, B2M, HMBS, HPRT1, OAZ1, ACTB, TBP, UBC, 18s_rRNA and GAPDH [24]) in the NFKB1 knockdown PBMC model was analyzed using the online tool RefFinder [25], which integrates the results of analyses performed by four algorithms: the comparative ΔCt method, BestKeeper, NormFinder, and GeNorm. Normalized relative quantities (NRQ) of CD200R1 and NFKB1 were calculated by the $2-\Delta\Delta Ct$ method [26]. The Coefficient of Variation (CV) of the obtained Ct values for GAPDH was calculated to assess the stability of GAPDH expression across our experimental conditions. The amplicon sizes for relevant qPCR products, validated by agarose gel electrophoresis, are provided in the legend of Table 1.

Chromatin immunoprecipitation (ChIP)-qPCR

ChIP experiments were conducted on PBMCs using the SimpleChIP Plus Sonication ChIP Kit (Cell Signaling Technology, USA) following the manufacturer's protocols. Cells were cross-linked with 37% formaldehyde (Sangon, Shanghai, China) for 10 min at room temperature and then quenched with 0.125 mol/L glycine. Chromatin was fragmented by sonication using an Ultrasonic Signal Transmitting Instrument (Xianou, Nanjing, China) equipped with a 1/8-inch diameter microprobe. Sonication parameters were adjusted as follows: 40% of the maximum power output with 1-second on/off pulses for a total of 8 min to achieve the desired fragment size of 200–1000 bp. In our pre-experiments, 30% power for 5 min and 30 min, as well as 40% power for 6 min, were found to be unsatisfactory (Figure S3A).

Sonicated chromatin was incubated overnight at 4 °C with ChIP-grade antibodies, including anti-NFKB1 (CST, #13586) and anti-CREB (CST, #9197) antibodies. Anti-Histone H3 (CST, #D2B12) served as the positive control, and anti-IgG (CST, #2729) as the negative control. The amount of antibody was fixed at 10 μL. For chromatin, the recommended amount was 5–10 μg. Comparative analysis showed that 10 μg of chromatin yielded better ChIP results compared to 5 μg (higher yield of IP DNA). The detailed information can be found on the manufacturer's website (https://www.cellsignal.com/

products/chip-kits/simplechip-plus-sonication-chromatin-ip-kit/56383) or obtained by contacting the manufacturer directly.

The antibody-chromatin complex was incubated with protein A beads at 4 ℃ for 2 h. This was followed by three washes using a low salt buffer, and a final wash with a high salt buffer. All materials were supplied in the SimpleChIP Plus Sonication Chromatin IP Kit. Following the washing regimen, the complex was exposed to an enzymatic digestion process involving 2 uL of proteinase K and 6 uL of 5 M NaCl at an elevated temperature of 65 °C for a period of 2 h. Purified DNA was extracted for qPCR analysis. The qPCR reaction was prepared with 10 µL SimpleChIP® Universal qPCR Master Mix, 2 µL 5 µM primers (sequences provided in Table 1), 20 ng of purified DNA and Nuclease-free H2O up to a final volume of 20 µl. The cycling procedure was set as follows: initial denaturation at 95℃ for 3 min, followed by 40 cycles of denaturation at 95℃ for 15 s and annealing/extension at 60℃ for 60 s. The qPCR was performed using an Applied Biosystems ABI-Q7 instrument. IgG was used as control and IP efficiency was compared based on index of the Percent Input, which was calculated following the formula below: Percent Input = 2% x 2(C[T] 2%Input Sample - C[T] IP Sample)

C[T] = CT = Average threshold cycle of PCR reaction.

Electrophoretic mobility shift assay (EMSA)

HEK293T cells were transfected with either the pcDNA3.1 vector or the NFKB1 overexpression plasmid. The overexpression plasmid was constructed using a pcDNA3.1 vector with a CMV promoter and the NFKB1 expression was verified via Western blot analysis (Supplementary Figure S1b). Total protein was extracted and quantified using the BCA Protein Assay Kit (Pierce Biotechnology, USA), with freshly extracted protein yielding a concentration of approximately 5 µg/µL.

The EMSA was performed using biotin 5'-end-labeled complementary oligonucleotides synthesized by Biosune (Shanghai, China; sequences in Table 3). Probes were prepared via annealing, followed by a binding reaction with double-stranded oligonucleotides. Through a systematic exploration of varying concentrations, our optimized condition for binding assays is 2 mg/mL protein and 0.2 µM probe. The incubation time was 30 min at 22℃, in accordance with the standard protocol (GS005, Beyotime). The optimal incubation mix included 2 µL of EMSA/Gel-Shift binding buffer (5X) (GS005, Beyotime), 4 µL of total extracted protein, and 4 µL of labeled probe. We employed a reported sequence with affinity to NFKB1 (GTA GGG GGC CTC CCC GGC TCG AGA TCC TAT G) [27] as the positive control. The negative control was the reaction mixture without protein. The reaction mixtures were separated with electrophoresis on a 5% nondenaturing polyacrylamide gel at a constant voltage of 80 V for 1 h at 4 °C. Subsequently, the DNA-protein complexes were transferred onto a nylon membrane. The membrane was irradiated with a handheld UV detector (EUV002, Beyotime) at a distance of 5–10 cm for at least 20 min.

The membrane was then blocked and washed, followed by incubation with streptavidin-conjugated horseradish peroxidase in accordance to manufacturer's instructions (https://www.beyotime.com/product/GS009.htm). Visualization was achieved using a chemiluminescent substrate. Chemiluminescent signals were obtained using a ChemiDoc MP system (Bio-Rad, USA) with exposure times set at 1s, 5s, 10s, and 30s. Images characterized by optimal clarity and minimal background noise were chosen for band comparison.

To address normalization, the grayscale value of each lane was divided by that of the positive control lane (with reported probe which can bind to NFKB1). For background subtraction, we first subtracted the grayscale values of the surrounding areas for each lane and then applied the background subtraction feature in Fiji to refine the measurements. For the statistical analysis of EMSA, ANOVA was used to compare the binding affinity ratios across different probes, based on normalized grayscale values.

Cell-based enzyme-linked immunosorbent assay (ELISA) of CD200R1

CD200R1 expression in PBMCs was quantified via a cell-based ELISA. Prior to seeding, 96-well plates were coated with poly-lysine, incubated at 37 °C for one hour and then quickly rinsed three times with 200 µL of PBS per

Table 3 5'-end-labelled complementary oligonucleotides for EMSA[a]

Name	Sequence	Positionb	
probe 1	GAGAGGAGAACCAATGAGCTGAGAGATAATTCAATCAATCTGCTTCCTC	-315	-267
probe 2	TATCTTGGACACGTTCAATGCCTTACTGTAAAGTTTGTCTGTGTACAGCAGAAGTGAGAGG	-370	-310
probe 3	CAAAGTAGATCAATATTCTGTTTTACTTTTTGGTGCAAGTTTAGACAAATCTGTTTATCTT	-425	-365
probe 4	TCAACCTGGAGAAAGCCTCTAAAAGTCATCATAATTGGGAAATTTACAAGGATGGGCCAAAGT	-482	-420
Positive control	GTAGGGGGCCTCCCCGGCTCGAGATCCTATG	/	/

[a] EMSA, Electrophoretic mobility shift assay

[b] Position, distance from translation initiation site

well each time. PBMCs were plated at a concentration of 4×104 cells per well (detailed seen in "Isolation and Culturing of Peripheral Blood Mononuclear Cells (PBMCs)" section and in "siRNA and Transfection" section). Following transfection with siRNA or a control sequence (detailed in the "siRNA and Transfection Protocol" section), cells were centrifuged at 1,000 rpm for 10 min using a Beckman Coulter Microplus Carrier adapted for rotor GH 3.8, designed for micro-titer plates. Subsequently, supernatants were aspirated and cells were fixed with a 4% paraformaldehyde solution for 30 min at ambient temperature.

After washing each well twice with 200 µL of PBS for 5 min per wash, non-specific binding sites were blocked by adding 5% BSA and incubating at room temperature for 1 h. The cells were then incubated with the anti-CD200R1 antibody (catalog: AF3414, R&D Systems) at a concentration of 0.5 µg/mL in 1% BSA in PBS at 4 °C overnight. The validity of the antibody for ELISA assay was confirmed by the manufacturer with recombinant CD200R1 protein (https://www.rndsystems.com/cn/products/human-cd200r1-antibody_af3414). We did not include specific controls in our experiment. After washing each well three times with 200 µL of PBS, allowing 5 min per wash, a horseradish peroxidase (HRP)-conjugated secondary antibody (A0181, Beyotime, Shanghai, China) was added at a 1:300 dilution in 3% BSA in PBS and incubated at room temperature for 1 h. The plate was then washed three times with 200 µL of PBS per well, each wash lasting 5 min. Afterwards, the plate was added with the substrate 3,3',5,5'-Tetramethylbenzidine (TMB) for reaction initiation. After incubation at room temperature for 15 min, the reaction was stopped by H_2SO_4. The absorbance at 450 nm was detected using an ELISA plate reader (Softmax 190, Molecular Devices). After the initial reading, the fixed cells were washed with 200 µL of PBS per well for 30 min and then stained with crystal violet. The reading for absorbance at 598 nm was recorded.

The expression level of CD200R1 was represented by the absorbance ratio of 450 nm/598 nm. Each experiment was performed in triplicate wells and independently repeated three times to ensure the reliability of the results. A series of experiments were carried out before the optimal condition was determined. The primary antibody concentration was set at 0.5 µg/mL, as per the manufacturer's recommendations. After evaluating a range of incubation times, the most suitable durations were found to be an overnight period at 4 °C for the primary antibody, 1 h at room temperature for the secondary antibody, and 15 min at room temperature for the TMB incubation.

Animals and treatments

This study was approved by the Animal Ethics Committee of Shanghai Ruijin hospital affiliated to Shanghai Jiaotong University School of Medicine on June 8, 2018, and the relevant approval document has been provided as an attachment. All animal procedures were conducted in strict adherence to the NIH guidelines and the "Guide for the Care and Use of Laboratory Animals" (8th Edition, 2011), along with our institutional guidelines for animal care and use. The Institutional Animal Care and Use Committee (IACUC) approval documentation is available upon reasonable request, subject to institutional policies and confidentiality considerations. Eight-week-old homozygous NFKB1-/- and NFKB1+/+ (B6,129NFKB11tm1Bal and B6,129 2/J; Jackson Laboratory, Bar Harbor, ME) mice were used in the experiments. The animals were group-housed, three or four per cage, with ad libitum access to food and water. They were maintained in a temperature-controlled environment at 22±2 °C with a 12:12 light-dark cycle, with lights on at 7:00 AM and off at 7:00 PM to provide a precise description of the animals' circadian rhythm. Regular health checks were conducted by veterinary staff, and all personnel were properly trained and certified.

Mice were randomly divided into four groups, (i) Saline/NFKB1+/+ group: 0.2 ml saline intraperitoneal (IP) injection in NFKB1+/+ mice; (ii) Saline/NFKB1-/- group: 0.2 ml saline IP injection in NFKB1-/- mice; (iii) MPTP/NFKB1+/+ group: 20 mg/kg MPTP IP injection in NFKB1+/+ mice; (iv) MPTP/NFKB1-/- group: 20 mg/kg MPTP IP injection in NFKB1-/- mice.

Prior to treatment, the mice underwent a pre-training phase involving a battery of behavioral tests, including the rotarod test, swim test, and traction test, over a period of five consecutive days (for detailed methodologies, refer to the Behavioral Test section). Following the pre-training phase, the animals received once-daily treatments of either saline or MPTP for five consecutive days, administered between 08:00 and 09:00 in the morning. Subsequently, the swim test and traction test were carried out on the 6th day after the ultimate treatment while the rotarod started on the next day posterior to the final administration, lasting for 6 days. The experimental animals were humanely euthanized at 7 days post-MPTP treatment (Figure S1a).

Each experimental group consisted of 12 mice. The sample size was determined using PASS 2021 software (for detailed methodologies, refer to the Statistic Analysis section). Six mice from each group were used for immunofluorescence, as detailed in the "Tissue Preparation" and "Immunofluorescence and Confocal Microscopy Analysis" section.

Tissue preparation

After completing behavioral testing, mice were anesthetized with 10% chloral hydrate intraperitoneally (300 mg/kg) [28]. Subsequently, the animals were subjected to intracardiac perfusion. They were first perfused with 100 mL of 0.9% saline solution at a rate of 2.5-3.0 mL/min, immediately followed by 100 mL of 4% paraformaldehyde (PFA, P0099, Beyotime) in 0.1 M phosphate buffer (PB; pH 7.4) at the same flow rate, the procedure which helps clear fluorescent substances and impurities from the blood, thus reducing autofluorescence. Brains were dissected and further fixed with 4% PFA for 48 h. The brains were then placed in 15%, 22.5% and 30% sucrose solutions at 4℃ until they sank to the bottom and afterwards embedded in optimal cutting temperature contained material. These blocks were stored in -80 °C freezer to prevent any degradation until ready for staining. Using a cryostat (Leica), coronal brain sections were obtained from the anterior region to the midbrain. The SN, located between 2.9 mm and 4.1 mm posterior to the bregma, was specifically targeted. To ensure complete coverage of the SN area and avoid missing any part of it, sections were harvested continuously until approximately 2.5 to 4.5 mm posterior to the bregma, as in reference [29]. These sections, sliced at a 20-um thickness, were transferred onto slides and subjected to air-drying at room temperature until securely adhered to the slides.

Immunofluorescence and confocal microscopy analysis

Brain sections were thoroughly rinsed with PBS three times for 5 min each, followed by permeabilization in PBS containing 0.5% Triton X-100 for 30 min and antigen retrieval using antigen retrieval solution (P0090, Beyotime) at pH 7.4 and room temperature for 5 min. After three additional PBS washes, sections were blocked with 5% BSA in TBST for 60 min at room temperature. Primary antibodies, anti-tyrosine hydroxylase (TH, AB152, Millipore, https://www.sigmaaldrich.cn/CN/en/product/mm/ab152) and anti-IBA1 (019-19741, Wako, https://labchem-wako.fujifilm.com/asia/product/detail/W01W0101-1974.html) were then applied. The anti-TH antibody has been verified by the manufacturer with positive controls including brain (corpus striatum, sympathetic nerve terminals) and adrenal glands, and a negative control using liver tissue. Additional validation of the antibody was performed using Western Blot analysis. This antibody has also been employed in multiple investigations for detecting dopaminergic neurons in the SN [30–32]. Examples of applying anti-Iba1 antibody in immunofluorescence were available on the Wako's website. Previous study has demonstrated its efficacy in detecting microglial activation in the SN of mice treated with MPTP [33]. These two antibodies have also been validated in our previous publication [34]. We did not include positive and negative controls in our study. The concentrations for these primary antibodies were chosen based on manufacturer recommendations and previous studies. For primary antibodies, we selected concentrations within the recommended range: 1:1000 for TH and 1:1000 for IBA1, as reported in prior studies (for IBA1 [35, 36]; for TH [37, 38]). The incubation was performed overnight at 4 °C (approximately 16 h). Afterwards, sections were washed three 5-minute PBS-T and then incubated with fluorescently labeled secondary antibodies Alexa Fluor 488 (Thermo Fisher Scientific, A-11008, 1:500) and Alexa Fluor 594 (Thermo Fisher Scientific, A-11012, 1:1000), and DAPI (2 μg/mL) for 1 h at room temperature. After five 5-minute PBST washes, the sections were mounted with ProLong™ Diamond Antifade Mountant (Thermo Fisher Scientific, P36961) to minimize photobleaching during imaging.

Confocal imaging was obtained using a Leica TCP SP8 laser scanning confocal microscope (Leica Biosystems) at a 40x magnification. We used a 405 nm semiconductor laser for blue fluorescence, a 488 nm argon laser for green fluorescence, and a 561 nm semiconductor laser for red fluorescence. The excitation and emission bandpass wavelengths were set at 405/420–480 nm (DAPI), 488/505–550 nm (Alexa Fluor 488), and 561/600–650 nm (Alexa Fluor 594). The pinhole size used was 1.00 Airy units (AU). The digital resolution of the acquired images was 1024×1024 pixels. To reduce photobleaching during observation, we also utilized a light shield to protect the samples. Imaging times were kept as short as possible for each session. Image acquisition was performed using the Leica Application Suite X. No post-processing steps were performed on the images, as we adjusted the focus and laser intensity before acquisition to meet the requirements for analysis. Image analysis was conducted with Fiji software (http://fiji.sc; software version 2.0.0-rc-68/1.52e). Quantitative analysis of TH-positive neurons or IBA1-positive microglia was conducted on the left side of the SN, consistently chosen for all animals to ensure uniformity and reproducibility. This decision was aligned with previous studies [29] and based on evidence that the MPTP mouse model induces bilateral lesions of dopaminergic neurons [39] and MPTP-induced Parkinsonism in humans is more symmetrical both in clinical manifestations and imaging findings compared to idiopathic Parkinson's disease [40, 41]. Cell counting was performed using Fiji software, totaling approximately 24 sections per mouse. We did not employ the stereological approach due to equipment limitation. To maintain accuracy, only cells with clearly identifiable nuclei which were TH-positive or IBA1-positive were included in the count. As for the estimation of the collective number of TH-positive neurons, Konigsmark formula was applied. The evaluation was performed independently by two researchers,

who underwent unified training to standardize the criteria for identifying TH-positive and IBA1-positive cells. The average of the independent counts was used for analysis.

Behavioral test

The literature describes various well-established behavioral tests for evaluating PD models, such as the rotarod [42–44], traction [45], swim [46, 47], open field [48], and pole tests [49, 50]. While effective in assessing motor impairments, each test has its own limitations, and the choice of tests can vary among research teams [51]. In our experiments, we used the traction, swim, and rotarod tests. The traction test assesses forelimb strength and coordination [52] but can be influenced by anxiety or motivation. The swim test measures endurance, motor coordination, and balance, though it may induce stress and miss subtle motor deficits. The rotarod test evaluates balance, coordination, and motor learning [53] but can be affected by factors like body weight and learning effects, and may not detect subtle gait or fine motor control issues. Despite these shortcomings, these tests are widely used in MPTP mouse models of PD, allowing comparison with existing research. Using multiple tests will reduce the risk of bias from any single method and offer a more comprehensive assessment of motor deficits.

The traction test involves gently holding mice by the base of their tails, allowing them to grasp a 5 mm diameter rope with their forelimbs. Upon having a secure grip, the mouse is released, and the time until falls is recorded. The mice were trained familiar with the test for five consecutive days before MPTP injection. The traction test was executed on the sixth day subsequent to the final MPTP injection.

Utilizing the YLS-4 C apparatus from the Academy of Medical Sciences in Shandong, China, up to five mice can be tested simultaneously on a five-lane rotating rod. The test was performed prior to the MPTP injection to establish baseline motor performance. Subsequently, the test was conducted daily for six consecutive days following the final MPTP injection [54]. During evaluation, the rod accelerates from 5 to 20 rpm over 2 min, and the duration each mouse remains on the rod is recorded. This test is repeated three times per mouse with 10-minute intervals to mitigate stress and fatigue.

The swim test was performed in a water tub (length, 40 cm; width, 25 cm; height, 25 cm), filled to a depth of 15 cm with warm water at a temperature of 27 ± 2 °C to avoid hypothermia. The mice stayed in the water tub twice daily for acclimatization for five consecutive days prior to experimentation. The test was executed on the sixth day subsequent to the final MPTP injection. The score system was set as follows: 0, the rear part dips while the head remains above water; 1, intermittent use of hind legs for swimming, with the body tilted to one side; 2, sporadic floating but predominantly engaged in swimming; 3, continuous swimming activity [55]. This test is repeated three times for each mouse, and average scores are calculated for statistical analysis.

Statistical analysis

Data normality was assessed using the Shapiro-Wilk test, and homogeneity of variances with Levene's test. The Student's t-test was used for normally distributed two-group comparisons, and the Mann-Whitney U test for non-normal distributions. For multiple group comparisons, one-way ANOVA was used if normality was met, otherwise, the Kruskal-Wallis H test served as the non-parametric alternative. Pairwise comparisons after ANOVA were conducted using the two-stage linear step-up procedure of Benjamini, Krieger, and Yekutieli to control the false discovery rate (FDR). Effect sizes were reported with p-values, using Cohen's d for two-group and Cohen's f for ANOVA comparisons. The correlation between CD200R1 and NFKB1 mRNA expression was evaluated across tissues from the GTEx database, using Spearman's correlation analysis in R (version 4.0.2), with $p < 0.05$ considered statistically significant.

Outliers were identified using the Robust Regression and Outlier Removal (ROUT) method with a Q value of 1% and were retained to preserve data integrity. Sensitivity analyses were conducted to assess the robustness of our findings by varying key parameters. This included testing the stability of results with and without outliers and employing alternative statistical models, such as both parametric and non-parametric tests. Post-hoc power analysis was performed using G*Power to evaluate whether the study had sufficient power to detect true effects, based on observed effect sizes, sample sizes, and the specified alpha level. A power above 0.8 (or 80%) indicates more reliable results. Sample size for animal experiments was determined using PASS 2021 software to achieve 90% power, with alpha level set at 0.05. Based on literature data [56], an initial sample size of 10 animals per group was chosen, with an additional 20% to account for exclusions, resulting in a final sample size of 12 per group.

Results

Defining the promoter region of CD200R1

We previously identified that the promoter region of human CD200R1 was located at 876 to 146 bp upstream of CD200R1 TIS [22]. In order to find the decisive transcription factors, the minimal core promoter region of CD200R1 needs to be identified. We therefore constructed nine different truncated constructs and transfected those constructs respectively into HEK293T cells (Fig. 1A). Then, luciferase activity was measured.

The results demonstrated that the absence of the distal promoter fragment from −1989 to -482 bp did not significantly decrease the promoter activity. However, the deletion of the −482 to -365 bp fragment (Mean Diff. = -7.027, Cohen's d = -5.83, 95% CI [-8.40, -5.65], $p<0.0001$) and −365 to -266 bp fragment (Mean Diff. = -5.601, Cohen's d = -4.64, 95% CI [-7.34, -3.86], $p<0.0001$), rather than the −266 to -146 bp fragment, led to a statistically significant downregulation of promoter activity. This reveals that a region within −482 to -267 bp incorporated the core promoter region of CD200R1. Post hoc analysis with an effect size (Cohen's f) of 3.46, an alpha level of 0.05, and a sample size of 4 per group, confirmed a power of 100%.

For further confirmation, we deleted the −482∼-267 bp from the long fragment of -1989 to -146 bp, and the results showed that the strong promoter activity of the −1989 to -146 bp fragment disappeared after deleting the −482 to -267 bp fragment (Fig. 1B). To summarize, the 482 to 267 bp upstream of the TIS forms the core region of the CD200R1 promoter and is sufficient to drive its transcription activity.

NFKB1 binds to the promoter of CD200R1 and regulates its transcription activity

Transcription factors with a functional DNA-binding domain can be recruited to the promoter regions. To identify the transcription factors involved in CD200R1 regulation, five strategies were used: (i) in silico analysis identifying the putative transcriptional factors able to bind to CD200R1 core promoter sequence using two different programs, UCSC CHIP-seq databases (http://genome.ucsc.edu/) and JARSPAR (http://jaspar.genereg.net/); (ii) excluding transcription factors that are not expressed in the brain based on the Human Protein atlas website (https://www.proteinatlas.org/); (iii) A total of six transcription factors shared by JARSPAR and UCSC chip-seq were shown in Fig. 2B and evaluated in further studies; (iv) the other 11 transcription factors in relation with either inflammation or neural functions were also enrolled for subsequent analysis (Fig. 2A and B); and (v) the reported two transcription factors of CD200R1 in mouse, C/EBPβ and PPARγ, were also evaluated in this study. Totally, 17 candidate transcription factors were included.

The regulatory function of these transcription factors on CD200R1 promoter activity was assessed by overexpression and knockdown experiments. Through overexpressing these candidate transcription factors in HEK293T, respectively, we found significant increases in CD200R1 promoter activity with increased levels of NFKB1 (Mean Diff. = 5.484, Cohen's d=21.03, 95% CI [5.12, 5.84], $p<0.0001$), CREB1 (Mean Diff. = 1.045, Cohen's d=4.01, 95% CI [0.70, 1.39], $p<0.0001$), and RelA (Mean Diff. = 1.041, Cohen's d=3.99, 95% CI [0.69, 1.39], $p<0.0001$) (Fig. 2C). Whereas in the monocyte cell line U937, NFKB1 was found to significantly elevate the CD200R1 promoter activity compared to pcDNA3.1 (Mean Diff. = 3.858, Cohen's d=9.48, 95% CI [3.132, 5.140], $p<0.0001$) (Fig. 2D). In the microglial cell line BV2, NFKB1 also significantly elevated CD200R1 promoter activity compared to pcDNA3.1 (Mean Diff. = 3.136, Cohen's d=8.03, 95% CI [2.132, 4.140], $p<0.0001$) (Fig. 2E).

Consistently, knocking down NFKB1 significantly reduced the activity of the CD200R1 promoter compared to the scramble control (Mean Diff. = -0.6531, Cohen's d = -11.28, 95% CI [-0.7821, -0.5242], $p<0.0001$) (Fig. 3A). Post hoc analysis, using an effect size (Cohen's d) of 11.28, an alpha level of 0.05, and a sample size of 6 per group, confirmed a power of 100%. To confirm their specific interaction, ChIP assay was performed and the CD200R1 promoter sequence was detected in the DNA-protein complex immunoprecipitated by the anti-NFKB1 antibody. The difference in DNA binding between NFKB1 and the IgG control was statistically significant (Mean Diff. = 13.09, Cohen's d=4.9, 95% CI [7.04, 19.15], $p=0.0039$) (Fig. 3B). Post hoc analysis, using an effect size (Cohen's d) of 4.9, an alpha level of 0.05, and a sample size of 3 per group, confirmed a power of 99.1%. We further performed EMSA experiments to examine the direct binding of NFKB1 to the CD200R1 promoter. Total proteins were extracted and incubated with biotin-labeled probes including a positive control oligonucleotide previously confirmed to bind NFKB1 and four distinct oligonucleotides corresponding to different segments of the CD200R1 promoter (probes 1–4, Table 3). As shown in Fig. 3C, the positive control exhibited clear binding with NFKB1. Neither probe 1 nor probe 2 showed any binding to NFKB1. Both probe 3 (binding intensity ratio: 1.16:1 relative to the positive control) and probe 4 (binding intensity ratio: 1.4:1 relative to the positive control) demonstrated that the binding affinity of probe 3, 4 with NFKB1 was similar as that of the positive control, indicating that NFKB1 binds specifically to the −482 to -365 bp region of the CD200R1 promoter (Fig. 3C).

NFKB1 positively regulates CD200R1 expression

Primary microglia from NFKB1+/+, NFKB1+/-, and NFKB1-/- mice were isolated to evaluate the regulatory role of NFKB1 on CD200R1 specifically in microglia. The coefficient of variation (CV) for GAPDH Ct values across different genotype groups was 2.769% (Fig. S3G), indicating minimal differences of GAPDH expression levels between primary microglial cells from different genotype mice [57]. Compared with the NFKB1+/+ group, an 84.1% reduction of CD200R1 mRNA level was observed in the NFKB1-/- group (Mean Diff.=-0.8411,

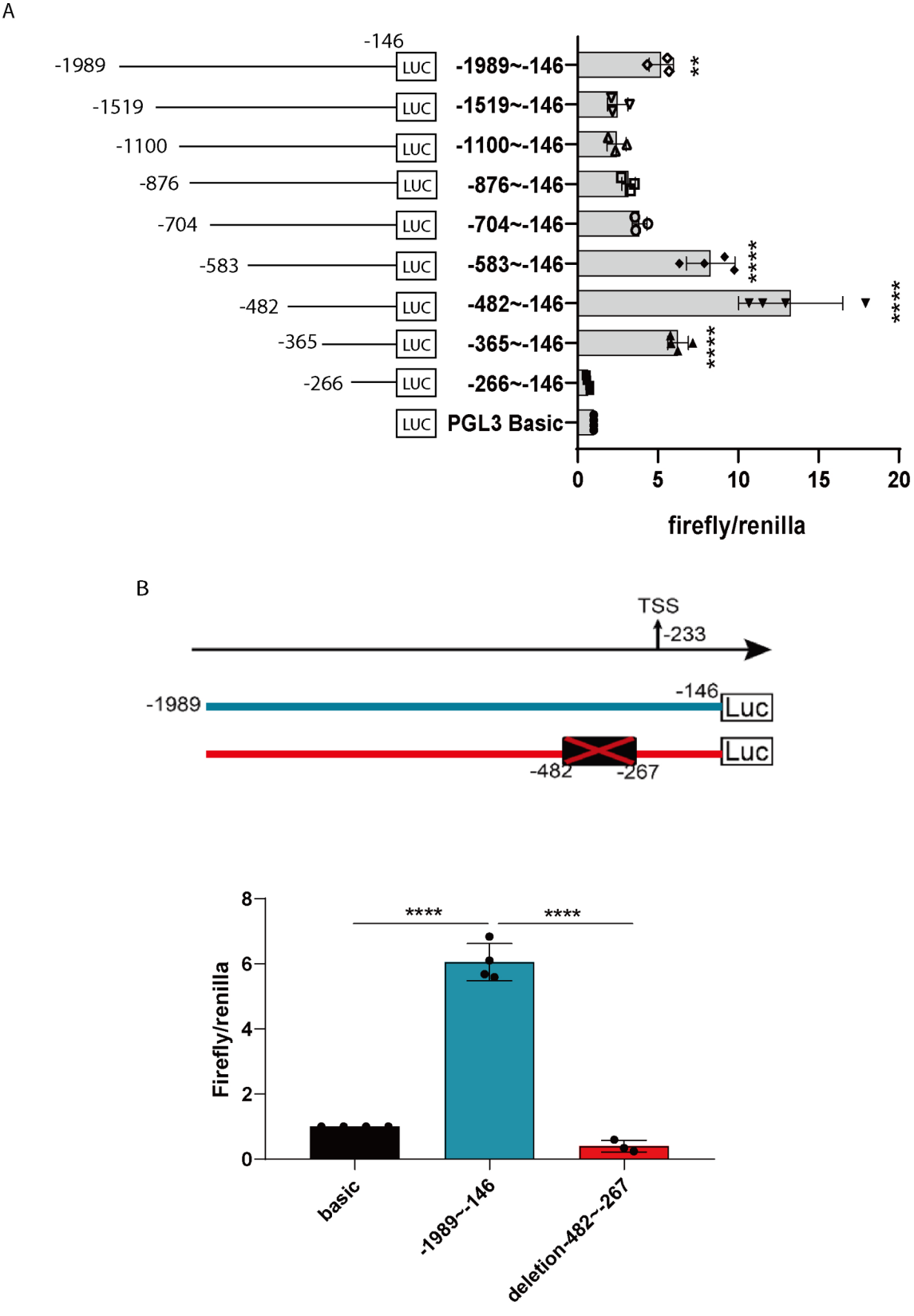

Fig. 1 (See legend on next page.)

(See figure on previous page.)

Fig. 1 Identification of the core promoter region of CD200R1. (**A**) Luciferase results for promoter screening. (Left) Schematic representation of dual-luciferase reporter constructs. The relative positions were calculated based on translation initiation site (ATG). The first base of ATG is referred to as 1 and the first upstream base of ATG is referred to as -1. The coverage of -1989 to -146 was studied. (Right) Luciferase activity detected 24 h after transfecting the different promoter plasmids with the Renilla plasmids in HEK293T cells. (**B**) Luciferase results for promoter confirmation. (Upper) Schematic representation of dual-luciferase reporter construct containing the long promoter region – 1989 to -146 and the construct with the sequence of -482 to -267 deleted. (Lower) Luciferase results of the corresponding plasmids transfected. Transfection and luciferase assay were carried out as described earlier. One-way ANOVA was used for statistical analysis. ** $P < 0.01$, **** $P < 0.0001$

Cohen's d=-8.94, 95% CI [-0.966, -0.716], $p<0.0001$), and a 57.13% reduction was observed in NFKB1+/- mice (Mean Diff.=-0.5713, Cohen's d=-7.79, 95% CI [-0.704, -0.439], $p=0.0001$) (Fig. 3D). Post hoc analysis, using an effect size (Cohen's f) of 5.57, an alpha level of 0.05, and 3 mice per group, confirmed a power of 100%. Furthermore, the mRNA levels of CD200R1 and NFKB1 were assessed in PBMCs from ten healthy individuals. PBMCs were chosen because of their similarity with microglia to some extent. Spearman correlation analysis showed a strong positive correlation between CD200R1 and NFKB1 expressions ($r=0.89091$, $p=0.00054$) (Fig. 3E). Besides, the correlation analysis from the GTEx database revealed a significant positive correlation of expression level between CD200R1 and NFKB1 ($R=0.521$, $p<2.2e-16$) (Fig. 3F). Specifically, in brain tissue, the correlation coefficient (R) is 0.315 with a p-value of 4.27e-28, indicating a significant positive correlation (Fig. 3G, Table S1). The correlation is also significant in 23 other tissues (red dots in Fig. 3G), including the small intestine and blood (detailed in Table S1). Silencing NFKB1 using siRNA significantly downregulated CD200R1 mRNA levels compared to the scramble control (Hodges-Lehmann estimate=-0.4163, 96.83% CI [-0.6312, -0.1554], p=0.0079, Fig. 3I-J), where ACTB and GAPDH were recommended as the reference genes with the RefFinder tool; and Cell-based ELISA suggested that the CD200R1 protein was also significantly reduced in the si-NFKB1 group compared to the scramble control (Mean Diff.=-4.338, Cohen's d=-1.275, 95% CI [-7.484, -1.191], $p=0.0150$) (Fig. 3K).

Reduced NFKB1 and CD200R1 expression in PBMCs of PD patients

Given that CD200R1 was significantly regulated by NFKB1, we examined the mRNA level of NFKB1 and CD200R1 in PBMCs from 44 PD patients and 45 age- and sex-matched healthy controls (Table 4). The CV for GAPDH Ct values in these PBMC samples was 2.291% (Figure S4E), suggesting the consistency of GAPDH under PD disease condition [57]. In both NFKB1 and CD200R1 expression analyses, significant reductions were observed in PD patients compared to healthy controls (NFKB1: Hodges-Lehmann estimate= -0.4000, 95% CI [-0.8400, -0.2100], $p<0.0001$; CD200R1: Hodges-Lehmann estimate = -0.3900, 95% CI [-0.9000, -0.1100], $p=0.0028$) (Fig. 4A-B). Post-hoc power analysis for CD200R1 (Cohen's d=1.12) showed a power of 99.97%, and for NFKB1 (Cohen's d=0.78), a power of 97.26%, both with an alpha level of 0.05 and sample size of 44 of PD group and 45 of healthy controls. Spearman correlation analysis showed a strong positive correlation between CD200R1 and NFKB1 expressions ($r=0.801$, $p<0.0001$) (Fig. 4C). These results further validated the regulatory role of NFKB1 on CD200R1 expression and their relevance in the development of PD.

Knockout of NFKB1 exacerbates MPTP-induced neurodegeneration, PD-related motor impairment and microglia activation

Our previous in vivo study has demonstrated that impairment of CD200-CD200R1 signaling would cause abnormal dopaminergic neurons loss and activation of microglia, participating in the pathogenesis of PD [15]. To evaluate the role of NFKB1 and CD200R1 in dopaminergic neuron loss and PD phenotype, we stained the midbrain coronal sections of MPTP-induced PD mice with an antibody against TH and counted the TH-immunoreactive (TH-ir) neurons in SN. Previously, we applied a dose of 30 mg/kg of MPTP to yield the animal model of PD [13, 58] and found that it could cause the loss of most dopaminergic neurons in SN (>60%) at 1week post-lesion. Therefore, in the present study, we used a sub-dose of MPTP (20 mg/kg) that was reported to result in moderate dopaminergic neurodegeneration in SN. This is also the sub-toxic dose of MPTP suggested by several groups [59, 60]. As expected, we observed that the sub-toxic dose of MPTP was able to induce moderate dopaminergic neurodegeneration in SN in NFKB+/+ mice (Fig. 5A-B). However, the TH-ir neurons were significantly reduced in NFKB1-/- mice (Fig. 5A-B). Detailed quantification is provided in Table S2, including average TH-positive neurons per animal (WT+saline: 3313, NFKB KO+saline: 3110, WT+20 mg/kg MPTP: 2879, NFKB KO+20 mg/kg MPTP: 617), range of neuron counts (WT+saline: 3064 to 3600, NFKB KO+saline: 2964 to 3360, WT+20 mg/kg MPTP: 2324 to 3144, NFKB KO+20 mg/kg MPTP: 432 to 864), total neurons counted (WT+saline: 19880, NFKB KO+saline: 18664, WT+20 mg/kg MPTP: 17276, NFKB KO+20 mg/kg MPTP: 3702), CV (WT+saline: 0.0234, NFKB KO+saline: 0.0183, WT+20 mg/kg MPTP: 0.0387, NFKB KO+20 mg/kg MPTP: 0.0932), and section thickness (20 μm). These results indicate an exacerbating effect of NFKB1 knockout on the degeneration

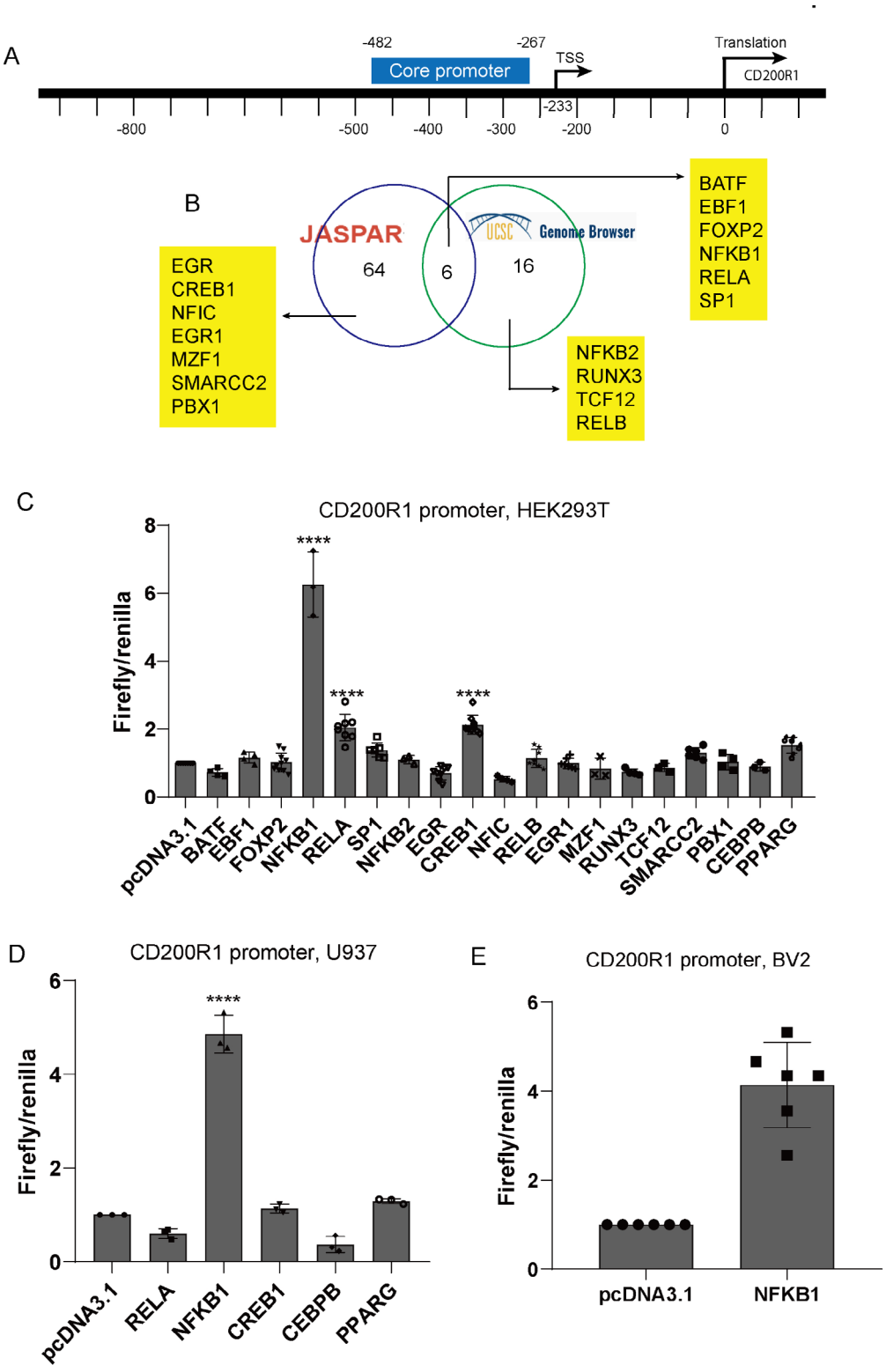

Fig. 2 NFKB1 is a potential transcription factor of CD200R1 and regulates its transcriptional activity. (**A**) Schematic representation of the CD200R1 core promoter sequence. The region covers the nucleotides from −482 to -146 based on the CD200R1 translation initiation site. (**B**) In silico prediction of the possible transcription factors. (**C**) Dual-luciferase assay results in human HEK293T cells transfected with the reporter construct containing the core promoter and overexpressing indicated transcription factors. (**D**) Dual-luciferase assay results in human U937 cells after overexpressing the CD200R1 core promoter and RELA, CREB1 and NFKB1, respectively. (**E**) Dual-luciferase assay results in microglia cell line BV2 transfected with the core promoter vector and NFKB1. One-way ANOVA was used for comparison. $^{**}P < 0.01$, $^{****}P < 0.0001$

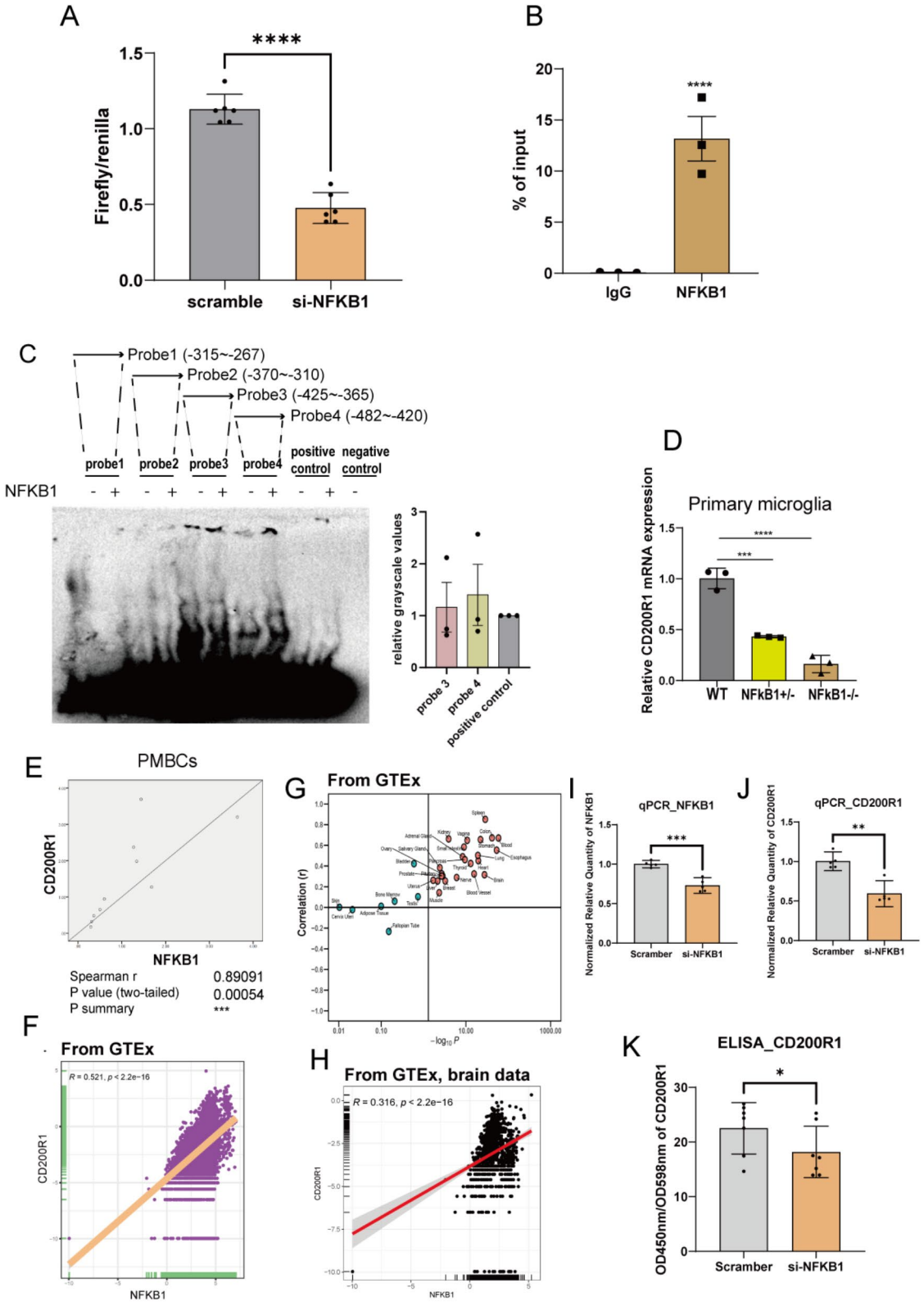

Fig. 3 (See legend on next page.)

(See figure on previous page.)

Fig. 3 NFKB1 binds to CD200R1 promoter and regulates CD200R1 expression at mRNA and protein levels. (**A**) Dual-luciferase assay results from HEK293T cells transfected with the core promoter vector and siRNA targeting NFKB1. (**B**) PBMC chromatin was immunoprecipitated with antibodies against CD200R1 and the related DNA fragments were quantified by RT-qPCR, using a primer set specific to core promoter region. (**C**) EMSA assay illustration after incubation of corresponding protein extraction with indicated probes. (**D**) CD200R1 mRNA levels detected by RT-qPCR in primary microglia from NFKB1+/+ and NFKB1-/- mice. (**E**) Spearman correlation analysis between NFKB1 and CD200R1 mRNA expressions in PBMCs from healthy individuals ($n=10$). (**F**) Sincorplot demonstrating the correlation between CD200R1 and NFKB1 expression levels across all tissues from the GTEx database. The Pearson correlation coefficient (r-value) was 0.521 and a significant positive correlation between the two genes was reached (*P*-value < 2.2e-16). (**G**) The respective correlation between CD200R1 and NFKB1 expression levels in different tissues from GTEx database. The tissues examined encompass a spectrum of biological systems, including Adipose Tissue, Adrenal Gland, Bladder, Blood, Blood Vessel, Bone Marrow, Brain, Breast, Cervix Uteri, Colon, Esophagus, Fallopian Tube, Heart, Kidney, Liver, Lung, Muscle, Nerve, Ovary, Pancreas, Pituitary, Prostate, Salivary Gland, Skin, Small Intestine, Spleen, Stomach, Testis, Thyroid, Uterus, and Vagina. Each circle represents one tissue, with the x-axis indicating the negative logarithm of the *p* value (-Log10 *p* value) and the y-axis indicating the correlation coefficient value. Strong correlations were observed in brain tissues ($r=0.316$, $p<2.2e\text{^-}16$). (**H**, **I**) Comparison of CD200R1 mRNA (**H**) and protein (**I**) levels in PBMCs with or without NFKB1 knockdown. Unpaired student test was used for statistical analysis. **$P<0.01$, **** $P<0.0001$

of dopaminergic neurons. Microglial activation was also evaluated. Staining of Iba1, a constitutive marker specially expressed on microglia showed the morphological changes of microglia (Fig. 5C). Besides, the total number of Iba1-positive cells in SN in MPTP/NFKB1-/- mice was significantly increased, compared with that in MPTP/NFKB1+/+ mice (Fig. 5C-D).

To evaluate whether the PD phenotype of MPTP/NFKB1-/- mice is consistent with the dopaminergic neuron loss in SN, we conducted swim test, traction test and rotarod test, which are routine tests applied in PD models to estimate the motor coordination. In swim test (Fig. 5E), several mice in the MPTP/NFKB1+/+ group exhibited a slight reduction of swim score in comparison with the untreated NFKB+/+ mice. However, the swim score in the MPTP-treated NFKB1-/- group was significantly lower than in both the untreated NFKB1-/- group (Mean rank difference = -21.54, $P<0.0001$, $q<0.0001$) and the MPTP-treated NFKB1+/+ group (Mean rank difference = -14.42, $P=0.0025$, $q=0.0027$). Results from traction test (Fig. 5F) suggested that MPTP/NFKB1-/- mice had a decreased strength as the hanging time was shorter than the MPTP/NFKB1+/+ group (Mean rank difference = -23.04, $p<0.0001$, $q<0.0001$). The rotarod test data includes measurements taken prior to the MPTP injection to establish baseline motor performance, followed by daily assessments for six consecutive days post-injection to evaluate the impact of the treatment on motor coordination and endurance (Fig. 5G). The results suggested that compared with their MPTP/NFKB1+/+ counterparts, MPTP +/ NFKB1-/- mice had a shorter latency before dropping. These results indicate that NFKB1 knockout can exacerbate the motor impairments triggered from MPTP.

Discussion

As the major CNS-resident immune cells, microglia are critically required for the initiation and maintenance of innate immune responses. It has been well-established that microglia activation acts as a central driver in neuroinflammation, one of the hallmarks of PD. The microglia CD200R1 and neuron/glia cells CD200 is one of the essential interactions for sustaining microglia in the resting state and prohibiting their activation [12]. A down-regulation of CD200R1 has been described in experimental models and patients of PD [13, 19] despite the mechanism underlying CD200R1 down-regulation in this setting remains yet to be discovered.

Based on our previous data, the CD200R1 down-regulation in PD was most likely to be attributable to the transcriptional change [22]. Regarding that gene turn on and off is controlled by the promoter and promoter activity is modulated by a series of transcription factors, we for the first time determined the core promoter region of human CD200R1 and searched for its potential binding partners. In our results, the core promoter region of CD200R1 was located between the 482 to 267 bp upstream of TIS and identified NFKB1 acted as its crucial transcription factor. We observed direct binding of NFKB1 to CD200R1 promoter and demonstrated the regulatory function of NFKB1 on CD200R1 transcription. Expression of CD200R1 was also significantly reduced in primary microglia from NFKB1 knock-out mice. It is worth mentioning that strong positive correlation between CD200R1 and NFKB1 levels was detected in PBMCs from healthy individuals and from the GTEX analysis, further suggesting NFKB1 exert significant regulation on CD200R1 levels. Therefore, it is proposed that decreased level of CD200R1 derived from NFKB1 defect could potentially lead to aggravated and unregulated microglia activation. Our results revealed significantly exacerbated and more obvious activated microglia but considerable loss of dopaminergic neurons in SN. Similarly, multiple reports in mice suggested that absence of NFKB1 could augment microglial pro-inflammatory responses after exposure to stimulation like pathogens, LPS and IFN-β [61–64]. As excessive and chronic microglia activation and neuroinflammation can contribute to progressive neuron damage, NFKB1 deficiency could possibly cause neurodegenerative disorder including PD. We discovered a significantly lower profile of NFKB1 in the PBMCs from PD patients, with reduced expression of CD200R1 and

Table 4 Demographic and clinical characteristics of controls and PD patients[a]

Value	Control	PD	*p*value[b]
	N=45	*N*=44	
Sex			0.608
Male, *n* (%)	22(48.9)	19(43.2)	
Female, *n* (%)	23(51.1)	25(56.8)	
Age, mean ± SD	64.70 ± 9.41	64.13 ± 9.78	0.441
Age of onset, mean ± SD	n.a.	61.05 ± 8.95	n.a.
Duration(year), *n* (%)			n.a.
≤ 2yr	n.a.	18(40.9)	
2-5yr	n.a.	17(38.6)	
5-10yr	n.a.	8(18.2)	
> 10yr	n.a.	1(2.3)	
Hoehn-Yahr stage, Median (IQR)	n.a.	1.77(0.81)	n.a.

[a] Attributes data are presented as mean ± SD; variables data are presented as numbers (%)

[b] the *p*-value of sex based on Chi-Squared Test and *p*-value of age based on student's t-test

positive correlation between the level of the two molecules. Likewise, decreased expression of NFKB1 has been demonstrated in Lewy Bodies Dementia (LBD) [65] and experimental models of dopaminergic neurodegeneration [66]. Moreover, the nucleotide variant rs28362491, a biallelic 4-nucleotides insertion/deletion within the NFKB1 promoter (-94 insertion/deletion ATTG), has long been linked with decreased NFKB1 transcript levels [67]. Recently, Álvarez's group reported a significant relevance between the above variant and risk of developing PD in male patients [68]. The evidence collectively supported NFKB1's value in homeostasis maintenance and the consequent neuroprotective effect.

Based on the findings of our studies and other research groups, NFKB1 shows potential in early diagnosis, disease monitoring, and treatment response prediction, particularly in its role in reflecting neuroinflammatory processes. To establish its clinical utility, it is essential to assess its specificity and sensitivity. The observed variability of NFKB1 expression in PD patients suggests that incorporating NFKB1 into a multimarker panel could improve diagnostic and prognostic accuracy. Longitudinal studies are needed to track NFKB1 levels over the course of PD, offering insights into disease progression and treatment efficacy. In addition, the translation of these findings into clinical practice presents several challenges, including the need for a more feasible assay beyond qPCR and extensive sample collection for the method standardization.

NFKB1 belongs to the NF-κB family which is composed of five members: c-Rel, RelA, RelB, NFKB1 and NFKB2. At the resting state, the NF-κB is sequestered in the cytoplasma by interacting with inhibitors of κB (IκB) family. Upon stimulation, IκB kinase (IKK) rapidly phosphorylates the IκB, releasing active NF-κB proteins to translocate into nucleus and thereby regulates a broad variety of gene transcriptions [69]. It is well investigated that NFKB1 participates in inflammation promotion through forming heterodimers with RelA while its anti-inflammatory profile is dependent on formation of homodimers [70]. Additionally, c-Rel has been reported to have neuroprotective effects, contributing to the diverse roles of NF-κB family members [71]. The homodimerized NFKB1 could negatively manipulate a broad range of pro-inflammatory molecules (e.g., MMP-13, CCL2 and CXCL10) [70] or activate the transcription of anti-inflammatory genes. Mosser and his colleagues previously demonstrated that NFKB1 was able to promote the transcription of anti-inflammatory cytokine IL-10 and the macrophages derived from the NFKB1 knockout mice exhibited an impaired production of IL-10 in response to the LPS [72]. In our study, the anti-inflammatory properties of NFKB1 were relied on its capacity to drive the transcription of CD200R1, extending the current understanding and shedding light on an alternative pathway where

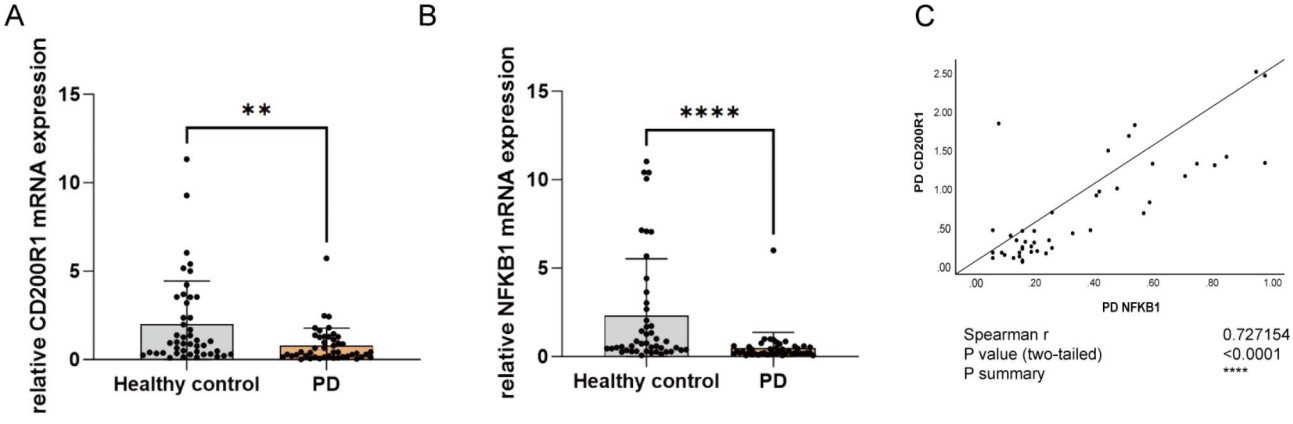

Fig. 4 Expression levels of NFKB1 and CD200R1 in PD patients. (**A**, **B**) CD200R1 (**A**) and NFKB1 (**B**) mRNA levels were assessed in PBMCs from PD patients (*n* = 44) with age- and sex-matched healthy controls (*n* = 45) by RT-PCR. Non-parameter analysis was used for between-group comparison. (**C**) Spearman correlation analysis between CD200R1 and NFKB1 mRNA expressions in PBMCs from PD population

NFKB1 could suppress inflammation through maintaining homeostasis of microglia.

As mentioned before, NFKB1 can regulate multiple genes and other molecules or pathways controlled by NFKB1 may also contribute to PD pathogenesis. To further investigate these multiple pathways related to NFKB1-CD200R1 axis, future studies should employ advanced methodological approaches. Systems biology and multi-omics studies, for example, can integrate large-scale datasets (e.g., genomics, transcriptomics, proteomics, and metabolomics) to construct and analyze network models of the NFKB1-CD200R1 axis and its related pathways. Additionally, in vivo models that capture more aspects of PD pathology, such as genetically engineered mouse models and iPSC-derived microglia-like cells, will be crucial for validating these interactions and their role in PD. These approaches will provide a deeper understanding of the complex regulatory networks involved in PD and could pave the way for novel therapeutic strategies.

Our study provides novel insights into the relationship between NFKB1 and CD200R1 across various tissues, emphasizing the critical role of this axis in immune regulation and neuroinflammation. We identified a significant positive correlation between NFKB1 and CD200R1 expression across several tissues, including the brain, blood, and gastrointestinal tract. Specifically, in blood (R=0.671, p-value=2.54e-59), this correlation aligns with our findings in PBMCs, indicating a consistent regulatory relationship between NFKB1 and CD200R1 in both central and peripheral immune cells. This suggests that the NFKB1-CD200R1 axis may play a crucial role in peripheral inflammation, potentially influencing CNS inflammation through systemic immune responses. Furthermore, the strong correlations observed in gastrointestinal tissues, such as the colon (R=0.672), stomach (R=0.656), and small intestine (R=0.584). The decreased NFKB1 in PD patient may cause the inflammatory responses in gastrointestinal tract. The microbiome-gut-brain axis is increasingly recognized as a critical factor in the pathogenesis of PD [74, 75]. These suggest gastrointestinal NFKB1-CD200R1 axis would join with the microbiome-gut-brain axis to contribute the pathogenesis of PD. To the best of our knowledge, no previous studies have specifically investigated the relationship between NFKB1 and CD200R1 in either normal individuals or PD patients. This study is therefore the first to provide data on the correlation between these two genes, highlighting the importance of the NFKB1-CD200R1 axis in PD pathophysiology.

Our study highlights the potential of targeting NFKB1 as a therapeutic approach for PD, though key challenges remain. Given the role of NFKB1 in regulating various factors and cellular processes, specific targeting without impacting other pathways or cellular function is complex. NFKB1 have been reported to inhibit EGFR transcription and suppress the progression of colon cancer [73]. Thus, targeting NFKB1 could lead to an increased risk of cancer. Specifically targeting CNS microglia may be a beneficial strategy to minimize potential widespread effects. Exploring methods for delivering NFKB1 modulators across the blood-brain barrier, such as using nanoparticles, could be particularly valuable [74]. In addition, exploring strategies like delivering NFKB1 modulators across the blood-brain barrier using nanoparticles [74–76] could minimize potential widespread effects. Moreover, determining the optimal dosage is crucial to balancing therapeutic benefits with side effects, and long-term NFKB1 modulation requires careful consideration due to its extensive role in cellular processes. Other alternative strategies could include focusing on downstream effectors of NFKB1, such as CD200R1, which may offer a more targeted approach to modulating neuroinflammation. Additionally, combining NFKB1 modulation with other therapeutic approaches, such as anti-inflammatory or neuroprotective agents, could enhance efficacy and reduce the risk of side effects.

Unlike other NF-κB family members including RelA, RelB and c-Rel, NFKB1 does not possess C-terminal transcriptional activation domains, sequences able to recruit and stabilize the general factors like TATA-binding protein which are crucial for transcription initiation [77]. As a consequence, NFKB1 can properly stimulate transcription only if partnered with the transactivation domain-containing co-regulators [70]. Therefore, it is of great research value to explore for the co-factors participating in NFKB1's regulation on CD200R1 expression in future study.

In our study, since primary human microglia are ethically and technically difficult to obtain and only allow low throughput studies, we employed PBMCs as a proxy for microglial cells. PBMCs share several morphological and functional similarities with microglia, including phagocytic activity, and have been used as surrogates for microglia in studies [78–80]. Additionally, research using the translocator protein (TSPO) as an immune cell marker found a strong positive correlation between TSPO levels in brain and blood cells in healthy individuals [81]. Another study reported that in patients with isolated rapid-eye-movement sleep behavior disorder (iRBD), a prodromal phenotype of synucleinopathy-related parkinsonism, monocyte Toll-like receptor 4 (TLR4) expression was positively associated with nigral immune activation [82]. These findings suggest that peripheral immune activity may reflect neuroinflammatory processes in the CNS. However, PBMCs and microglia differ significantly in ontogeny and kinetics. Microglia arise from yolk sac progenitors during primitive hematopoiesis, while

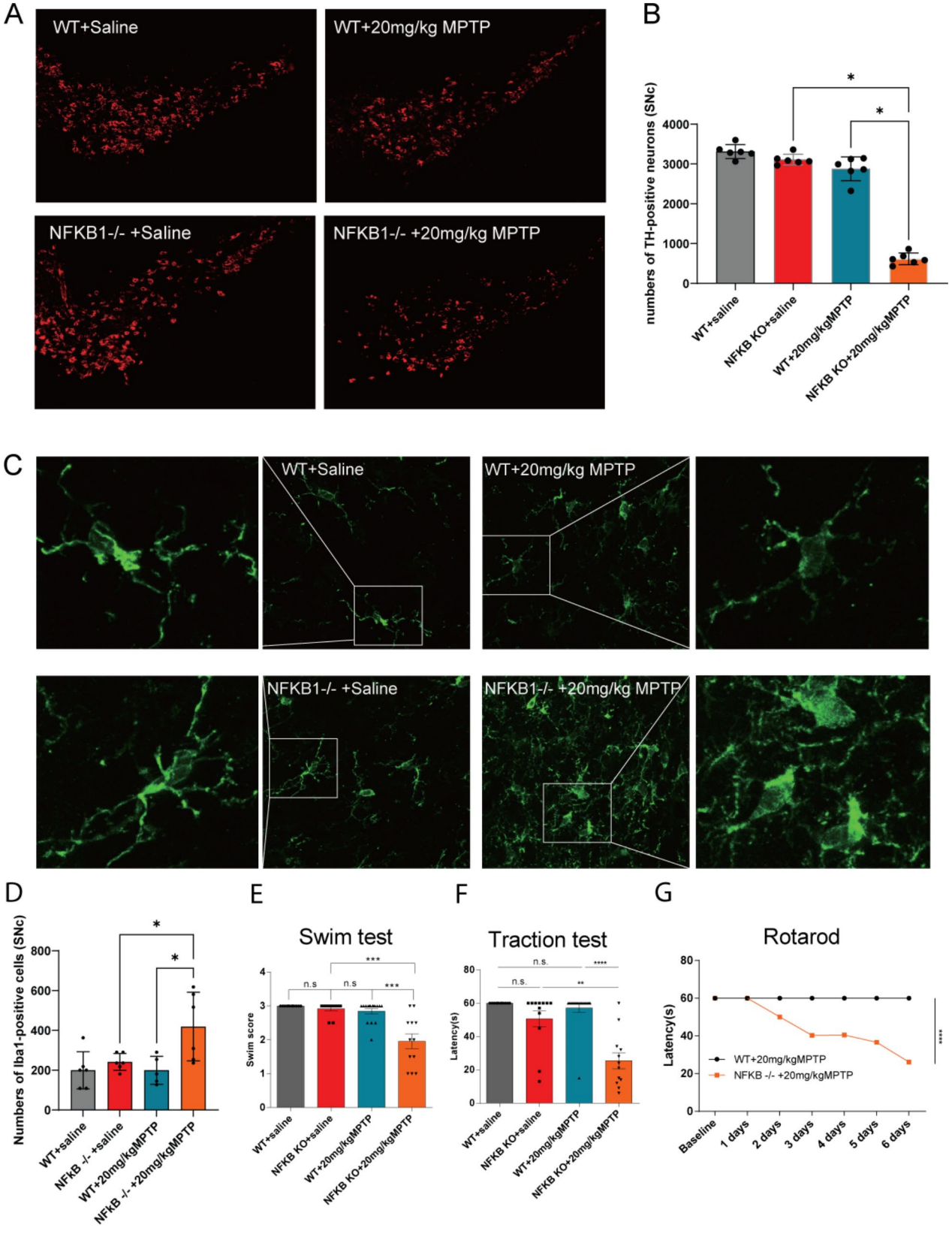

Fig. 5 (See legend on next page.)

(See figure on previous page.)

Fig. 5 Loss of NFKB1 exacerbates PD phenotypes in MPTP-treated mice. (**A-B**). Animals (6 mice per group) were sacrificed on day 7 post MPTP injection and sections of SN were immunostained with antibody against tyrosine hydroxylase (TH). Representative illustrations were presented (**A**) and stereological cell counts were conducted (**B**) (Right, $n = 6$/group). (**C-D**) Characteristic staining of microglia was displayed (**C**) using antibody targeting Ibal and the Iba1-positive cells were enumerated (**D**) in SN sections from mice mentioned before. Double-blinded procedure was adopted and data is presented as mean ± S.E.M. (**E-G**) Behavioral examination results comparing MPTP-administrated mice with or without NFKB1 knockout. Swim test (**E**) and traction test (**F**) was performed on the 6th day subsequent to the final injection while the rotarod test (**G**) was conducted for 6 consecutive days after the last administration. There were 12 mice in each group. Data was presented as mean ± standard error and differences were analyzed by one-way analysis of variance followed by least significant difference post hoc test. *$p < 0.05$, **$p < 0.01$, ***$p < 0.001$, ****$p < 0.0001$

PBMCs derive from hematopoietic myeloid progenitors during definitive hematopoiesis in the aorta-gonad-mesonephros (AGM) region [83]. In addition, unlike resident CNS microglia, PBMCs circulate throughout the body, encountering diverse systemic signals, pathogens, and cytokines, leading to potentially divergent immune responses. Therefore, extrapolating CNS-specific changes from PBMC findings should be approached with caution. To address this limitation, we recommend using models that more closely mimic microglia, such as microglia-like cells derived from induced pluripotent stem cells (iPSCs), which may provide a more accurate representation of microglial behavior and insights into the NFKB1-CD200R1 axis in CNS inflammation.

In our study, we employed the MPTP-induced PD model, a well-established and widely utilized model in PD research due to its robust ability to induce dopaminergic neurodegeneration. This model remains a valuable tool for studying neuroinflammation in PD, which is the primary focus of our research and a process recognized as critical in the pathogenesis of the disease [84, 85]. However, PD is a multifactorial condition with diverse etiologies, including genetic variants, neuroinflammation, protein aggregation, excitotoxicity, and mitochondrial dysfunction. we acknowledge that the MPTP model does not fully replicate the complete spectrum of PD pathology observed in humans. For instance, it lacks the formation of Lewy bodies, which are characteristic of many PD cases, and it is less effective in modeling non-motor symptoms such as mood disorders. Additionally, the neurodegeneration induced by MPTP occurs more rapidly compared to the chronic and progressive nature of neurodegeneration in human PD, posing challenges when attempting to extrapolate findings to clinical settings. Despite these limitations, our previous investigations have demonstrated decreased levels of CD200 and CD200R1 in the brains of MPTP-treated mice [13], supporting the suitability of the MPTP paradigm for exploring the regulatory mechanisms of CD200R1. Furthermore, similar findings in 6-OHDA-lesioned rats [15] corroborate the significance of this pathway in PD pathology. However, it is important to note that mouse models, including the MPTP model, represent a simplified version of the complex, multifactorial nature of human PD, which may limit the generalizability of findings to the broader patient population. In recognizing these limitations, we emphasize the need for complementary models to provide a more comprehensive understanding of PD. Genetic models of PD, for example, offer valuable insights into the hereditary components of the disease, enhancing our understanding of the genetic mutations that contribute to PD pathogenesis. Additionally, α-syn overexpression models are crucial for studying Lewy body pathology, a hallmark of PD that is absent in the MPTP model. These alternative models complement the MPTP model by addressing aspects of PD pathology that toxin-induced models cannot replicate, such as chronic neurodegeneration, non-motor symptoms, and protein aggregation.

We acknowledge that a more comprehensive design in some experiment could potentially lead to more convincing outcomes. For assays with antibodies, incorporating additional positive and negative controls to validate the antibodies could further ensure reliable examination, although these antibodies were already evaluated by the supplier or previous studies. As to normalization for qPCR analysis, pre-assessing stability of reference genes across conditions and selecting multiple reference genes could be implemented for enhanced trustworthiness. In terms of behavioral experiments, although our behavioral tests could effectively assess motor function of mice, application of additional tests like the open field and pole tests could provide a more thorough evaluation. Lastly, stereological methods for cell-counting in immunostaining assay will offer greater accuracy compared with the traditional method.

Conclusions

Generally, little has been known about the impact of NFKB1 on PD pathogenesis. Our present study demonstrated that NFKB1 was critically required in the regulation of CD200R1 transcription. The decrease of NFKB1 may contribute to PD progression by impairing the expression of CD200R1 and thereby amplifying the activation of microglia. These lines of evidence reasonably implicate NFKB1 could possibly serve as a PD biomarker and therapeutic target for drug development, deserving additional exploration in large patient cohorts and population across different disease stages.

Abbreviations

TIS	Translation initiation site
PD	Parkinson's disease

MPTP	1-Methyl-4-phenyl-1,2,3,6-tetrahydropyridine
SN	Substantia nigra
CNS	Central nervous system
TNF-α	Tumor necrosis factor-alpha
IFN-γ	Interferon-gamma
AD	Alzheimer's disease
PBMCs	Peripheral blood mononuclear cells
siRNA	Small interfering RNA
DMEM	Dulbecco's modified eagle medium
RPMI 1640 Medium	Roswell Park Memorial Institute 1640 Medium
FBS	Fetal Bovine Serum
ChIP	Chromatin immunoprecipitation
EMSA	Electrophoretic mobility shift assay
ELISA	Cell-based enzyme-linked immunosorbent assay
PBS	Phosphate-buffered saline

Supplementary Information

The online version contains supplementary material available at https://doi.org/10.1186/s12974-024-03231-3.

Supplementary Material 1

Acknowledgements
The authors thank all the patients and healthy controls participating in the study. We would also like to thank TopEdit (www.topeditsci.com) for its linguistic assistance during the preparation of this manuscript.

Author contributions
JD designed and supervised the study. JD, YS and SL wrote the manuscript. SL, RS and YS performed experiments and analyzed data. LH, YW and WX was involved in the data analysis. SL and FF generated cell lines transfected with the core promoter region. HP and XW performed bioinformatics analysis. XZ, LH, YZ and YS recruited participants and collected blood samples. All authors read and approved the final manuscript.

Funding
This study was supported by National Natural Science Foundation of China (82101324, 82171427 and 82101476).

Data availability
No datasets were generated or analysed during the current study.

Declarations

Ethics approval and consent to participate
All the procedures in this study were approved by the ethics committees of Shanghai Ruijin hospital affiliated to Shanghai Jiaotong University School of Medicine, and written informed consent was obtained from all patients.

Consent for publication
Not applicable.

Competing interests
The authors declare no competing interests.

Author details
[1]Department of Neurology, Institute of Neurology, Ruijin Hospital, Shanghai Jiaotong University School of Medicine, Shanghai, China
[2]Institute of Aging & Tissue Regeneration, Renji Hospital, Shanghai Jiao Tong University School of Medicine, No. 160 Pujian Road, Shanghai 200135, China
[3]Department of Aging, Ruijin Hospital, Shanghai Jiaotong University School of Medicine, Shanghai, China
[4]Maternity and child care centers, Fuzhou, Fujian, China

Received: 9 May 2024 / Accepted: 10 September 2024
Published online: 18 September 2024

References

1. Poewe W, Seppi K, Tanner CM, Halliday GM, Brundin P, Volkmann J, et al. Parkinson disease. Nat Rev Dis Primers. 2017;3:17013.
2. Dobbs RJ, Charlett A, Purkiss AG, Dobbs SM, Weller C, Peterson DW. Association of circulating TNF-alpha and IL-6 with ageing and parkinsonism. Acta Neurol Scand. 1999;100:34–41.
3. Mogi M, Harada M, Kondo T, Riederer P, Inagaki H, Minami M, et al. Interleukin-1 beta, interleukin-6, epidermal growth factor and transforming growth factor-alpha are elevated in the brain from parkinsonian patients. Neurosci Lett. 1994;180:147–50.
4. Selikhova MV, Kushlinskii NE, Lyubimova NV, Gusev EI. Impaired production of plasma interleukin-6 in patients with Parkinson's disease. Bull Exp Biol Med. 2002;133:81–3.
5. Brodacki B, Staszewski J, Toczyłowska B, Kozłowska E, Drela N, Chalimoniuk M, et al. Serum interleukin (IL-2, IL-10, IL-6, IL-4), TNFalpha, and INFgamma concentrations are elevated in patients with atypical and idiopathic parkinsonism. Neurosci Lett. 2008;441:158–62.
6. Halliday GM, Stevens CH. Glia: initiators and progressors of pathology in Parkinson's disease. Mov Disord. 2011;26:6–17.
7. Iannaccone S, Cerami C, Alessio M, Garibotto V, Panzacchi A, Olivieri S, et al. In vivo microglia activation in very early dementia with Lewy bodies, comparison with Parkinson's disease. Parkinsonism Relat Disord. 2013;19:47–52.
8. Hickman S, Izzy S, Sen P, Morsett L, Khoury E. Microglia in neurodegeneration. Nat Neurosci. 2018;21:1359–69.
9. Subramaniam SR, Federoff HJ. Targeting Microglial Activation States as a Therapeutic Avenue in Parkinson's Disease. Front Aging Neurosci. 2017; 9.
10. Casali BT, Reed-Geaghan EG. Microglial Function and Regulation during Development, Homeostasis and Alzheimer's Disease. Cells. 2021; 10.
11. Hoek RM, Ruuls SR, Murphy CA, Wright GJ, Goddard R, Zurawski SM, et al. Down-regulation of the macrophage lineage through interaction with OX2 (CD200). Science. 2000;290:1768–71.
12. Manich G, Recasens M, Valente T, Almolda B, González B, Castellano B. Role of the CD200-CD200R Axis during Homeostasis and Neuroinflammation. Neuroscience. 2019;405:118–36.
13. Ren Y, Ye M, Chen S, Ding J. CD200 inhibits inflammatory response by promoting KATP Channel Opening in Microglia Cells in Parkinson's Disease. Med Sci Monit. 2016;22:1733–41.
14. Xie X, Luo X, Liu N, Li X, Lou F, Zheng Y, et al. Monocytes, microglia, and CD200-CD200R1 signaling are essential in the transmission of inflammation from the periphery to the central nervous system. J Neurochem. 2017;141:222–35.
15. Zhang S, Wang XJ, Tian LP, Pan J, Lu GQ, Zhang YJ, et al. CD200-CD200R dysfunction exacerbates microglial activation and dopaminergic neurodegeneration in a rat model of Parkinson's disease. J Neuroinflammation. 2011;8:154.
16. Wang XJ, Zhang S, Yan ZQ, Zhao YX, Zhou HY, Wang Y, et al. Impaired CD200-CD200R-mediated microglia silencing enhances midbrain dopaminergic neurodegeneration: roles of aging, superoxide, NADPH oxidase, and p38 MAPK. Free Radic Biol Med. 2011;50:1094–106.
17. Rabaneda-Lombarte N, Serratosa J, Bové J, Vila M, Saura J, Solà C. The CD200R1 microglial inhibitory receptor as a therapeutic target in the MPTP model of Parkinson's disease. J Neuroinflammation. 2021;18:88.
18. Wang L, Liu Y, Yan S, Du T, Fu X, Gong X, et al. Disease Progression-Dependent expression of CD200R1 and CX3CR1 in mouse models of Parkinson's Disease. Aging Dis. 2020;11:254–68.
19. Luo XG, Zhang JJ, Zhang CD, Liu R, Zheng L, Wang XJ, et al. Altered regulation of CD200 receptor in monocyte-derived macrophages from individuals with Parkinson's disease. Neurochem Res. 2010;35:540–7.
20. Dentesano G, Straccia M, Ejarque-Ortiz A, Tusell JM, Serratosa J, Saura J, et al. Inhibition of CD200R1 expression by C/EBP β in reactive microglial cells. J Neuroinflammation. 2012;9:165.
21. Dentesano G, Serratosa J, Tusell JM, Ramón P, Valente T, Saura J, et al. CD200R1 and CD200 expression are regulated by PPAR-γ in activated glial cells. Glia. 2014;62:982–98.
22. Lin S, He L, Shen R, Fang F, Pan H, Zhu X, et al. Identification of the CD200R1 promoter and the association of its polymorphisms with the risk of Parkinson's disease. Eur J Neurol. 2020;27:1224–30.
23. Yang X, Lou Y, Liu G, Wang X, Qian Y, Ding J, et al. Microglia P2Y6 receptor is related to Parkinson's disease through neuroinflammatory process. J Neuroinflammation. 2017;14:38.
24. He Y, Yu S, Bae E, Shen H, Wang Y. Methamphetamine alters reference gene expression in Nigra and striatum of adult rat brain. Neurotoxicology. 2013;39:138–45.

25. Xie F, Wang J, Zhang B. RefFinder: a web-based tool for comprehensively analyzing and identifying reference genes. Funct Integr Genomics. 2023;23:125.
26. Hellemans J, Mortier G, De Paepe A, Speleman F, Vandesompele J. qBase relative quantification framework and software for management and automated analysis of real-time quantitative PCR data. Genome Biol. 2007;8:R19.
27. Coleman TA, Kunsch C, Maher M, Ruben SM, Rosen CA. Acquisition of NFKB1-selective DNA binding by substitution of four amino acid residues from NFKB1 into RelA. Mol Cell Biol. 1993;13:3850–9.
28. Xiong R, Wang Z, Zhao Z, Li H, Chen W, Zhang B, et al. MicroRNA-494 reduces DJ-1 expression and exacerbates neurodegeneration. Neurobiol Aging. 2014;35:705–14.
29. Niu M, Zhao F, Bondelid K, Siedlak SL, Torres S, Fujioka H, et al. VPS35 D620N knockin mice recapitulate cardinal features of Parkinson's disease. Aging Cell. 2021;20:e13347.
30. Alarcon-Gil J, Sierra-Magro A, Morales-Garcia JA, Sanz-SanCristobal M, Alonso-Gil S, Cortes-Canteli M et al. Neuroprotective and Anti-Inflammatory Effects of Linoleic Acid in Models of Parkinson's Disease: The Implication of Lipid Droplets and Lipophagy. Cells. 2022; 11.
31. Verma DK, Ghosh A, Ruggiero L, Cartier E, Janezic E, Williams D et al. The SUMO Conjugase Ubc9 Protects Dopaminergic Cells from Cytotoxicity and Enhances the Stability of α-Synuclein in Parkinson's. Disease Models eNeuro. 2020; 7.
32. Lee JY, Wang ZJ, Moscatello A, Kingsbury C, Cozene B, Farooq J, et al. Inflammatory gut as a pathologic and therapeutic target in Parkinson's disease. Cell Death Discov. 2022;8:396.
33. García-Domínguez I, Veselá K, García-Revilla J, Carrillo-Jiménez A, Roca-Ceballos MA, Santiago M, et al. Peripheral inflammation enhances Microglia Response and Nigral Dopaminergic Cell Death in an in vivo MPTP Model of Parkinson's Disease. Front Cell Neurosci. 2018;12:398.
34. Lin Z, Chen C, Yang D, Ding J, Wang G, Ren H. DJ-1 inhibits microglial activation and protects dopaminergic neurons in vitro and in vivo through interacting with microglial p65. Cell Death Dis. 2021;12:715.
35. Hijioka M, Futokoro R, Ohto-Nakanishi T, Nakanishi H, Katsuki H, Kitamura Y. Microglia-released leukotriene B_4 promotes neutrophil infiltration and microglial activation following intracerebral hemorrhage. Int Immunopharmacol. 2020;85:106678.
36. Maeda T, Nagata K, Yoshida Y. Exogenous l-DOPA induce no dopamine immuno-reactivity in striatal astroglias and microglias of adult rats with extensive nigro-striatal dopaminergic denervation. Neurosci Lett. 2008;433:255–8.
37. Giguère N, Delignat-Lavaud B, Herborg F, Voisin A, Li Y, Jacquemet V, et al. Increased vulnerability of nigral dopamine neurons after expansion of their axonal arborization size through D2 dopamine receptor conditional knockout. PLoS Genet. 2019;15:e1008352.
38. Huang Z, Si W, Li X, Ye S, Liu X, Ji Y, et al. Moxibustion protects dopaminergic neurons in Parkinson's Disease through Antiferroptosis. Evid Based Complement Alternat Med. 2021;2021:6668249.
39. Sedelis M, Schwarting RK, Huston JP. Behavioral phenotyping of the MPTP mouse model of Parkinson's disease. Behav Brain Res. 2001;125:109–25.
40. Snow BJ, Vingerhoets FJ, Langston JW, Tetrud JW, Sossi V, Calne DB. Pattern of dopaminergic loss in the striatum of humans with MPTP induced parkinsonism. J Neurol Neurosurg Psychiatry. 2000;68:313–6.
41. Hobson DE. Asymmetry in parkinsonism, spreading pathogens and the nose. Parkinsonism Relat Disord. 2012;18:1–9.
42. Lin MW, Lin CC, Chen YH, Yang HB, Hung SY. Celastrol Inhibits Dopaminergic Neuronal Death of Parkinson's Disease through Activating Mitophagy. Antioxid (Basel). 2019; 9.
43. Lin JG, Chen CJ, Yang HB, Chen YH, Hung SY. Electroacupuncture Promotes Recovery of Motor Function and Reduces Dopaminergic Neuron Degeneration in Rodent Models of Parkinson's Disease. Int J Mol Sci. 2017; 18.
44. Roostalu U, Salinas CBG, Thorbek DD, Skytte JL, Fabricius K, Barkholt P et al. Quantitative whole-brain 3D imaging of tyrosine hydroxylase-labeled neuron architecture in the mouse MPTP model of Parkinson's disease. Dis Model Mech. 2019; 12.
45. Jiang Z, Yin X, Wang M, Wang Y, Li F, Gao Y, et al. β-Hydroxybutyrate alleviates pyroptosis in MPP(+)/MPTP-induced Parkinson's disease models via inhibiting STAT3/NLRP3/GSDMD pathway. Int Immunopharmacol. 2022;113:109451.
46. Datta I, Mekha SR, Kaushal A, Ganapathy K, Razdan R. Influence of intranasal exposure of MPTP in multiple doses on liver functions and transition from non-motor to motor symptoms in a rat PD model. Naunyn Schmiedebergs Arch Pharmacol. 2020;393:147–65.
47. Cunha MP, Pazini FL, Lieberknecht V, Budni J, Oliveira Á, Rosa JM, et al. MPP(+)-Lesioned mice: an experimental model of motor, emotional, Memory/Learning, and Striatal Neurochemical dysfunctions. Mol Neurobiol. 2017;54:6356–77.
48. Rinaldi F, Seguella L, Gigli S, Hanieh PN, Del Favero E, Cantù L, et al. inPentasomes: an innovative nose-to-brain pentamidine delivery blunts MPTP parkinsonism in mice. J Control Release. 2019;294:17–26.
49. Zhou T, Zhu M, Liang Z. (-)-Epigallocatechin-3-gallate modulates peripheral immunity in the MPTP-induced mouse model of Parkinson's disease. Mol Med Rep. 2018;17:4883–8.
50. Hwang DJ, Kwon KC, Song HK, Kim KS, Jung YS, Hwang DY, et al. Comparative analysis of dose-dependent neurotoxic response to 1-methyl-4-phenyl-1,2,3,6-tetrahydropyridine in C57BL/6 N mice derived from three different sources. Lab Anim Res. 2019;35:10.
51. Prasad EM, Hung SY. Behavioral Tests in Neurotoxin-Induced Animal Models of Parkinson's Disease. Antioxid (Basel). 2020; 9.
52. Wang W, Yang Y, Ying C, Li W, Ruan H, Zhu X, et al. Inhibition of glycogen synthase kinase-3beta protects dopaminergic neurons from MPTP toxicity. Neuropharmacology. 2007;52:1678–84.
53. Monville C, Torres EM, Dunnett SB. Comparison of incremental and accelerating protocols of the rotarod test for the assessment of motor deficits in the 6-OHDA model. J Neurosci Methods. 2006;158:219–23.
54. Chen Y, Zhang Y, Li L, Hölscher C. Neuroprotective effects of geniposide in the MPTP mouse model of Parkinson's disease. Eur J Pharmacol. 2015;768:21–7.
55. Haobam R, Sindhu KM, Chandra G, Mohanakumar KP. Swim-test as a function of motor impairment in MPTP model of Parkinson's disease: a comparative study in two mouse strains. Behav Brain Res. 2005;163:159–67.
56. Sengupta T, Vinayagam J, Nagashayana N, Gowda B, Jaisankar P, Mohanakumar KP. Antiparkinsonian effects of aqueous methanolic extract of Hyoscyamus niger seeds result from its monoamine oxidase inhibitory and hydroxyl radical scavenging potency. Neurochem Res. 2011;36:177–86.
57. Shechtman O. The Coefficient of Variation as an Index of Measurement Reliability. In: Doi S and Williams G, Editors, editors. Methods of Clinical Epidemiology. 2013. pp. 39–49.
58. Dou F, Chu X, Zhang B, Liang L, Lu G, Ding J, et al. EriB targeted inhibition of microglia activity attenuates MPP(+) induced DA neuron injury through the NF-κB signaling pathway. Mol Brain. 2018;11:75.
59. Saporito MS, Brown EM, Miller MS, Carswell S. CEP-1347/KT-7515, an inhibitor of c-jun N-terminal kinase activation, attenuates the 1-methyl-4-phenyl tetrahydropyridine-mediated loss of nigrostriatal dopaminergic neurons in vivo. J Pharmacol Exp Ther. 1999;288:421–7.
60. Chen JY, Hsu PC, Hsu IL, Yeh GC. Sequential up-regulation of the c-fos, c-jun and bax genes in the cortex, striatum and cerebellum induced by a single injection of a low dose of 1-methyl-4-phenyl-1,2,3,6-tetrahydropyridine (MPTP) in C57BL/6 mice. Neurosci Lett. 2001;314:49–52.
61. Cheng CS, Feldman KE, Lee J, Verma S, Huang DB, Huynh K, et al. The specificity of innate immune responses is enforced by repression of interferon response elements by NF-κB p50. Sci Signal. 2011;4:ra11.
62. Harris TH, Wilson EH, Tait ED, Buckley M, Shapira S, Caamano J, et al. NF-kappaB1 contributes to T cell-mediated control of Toxoplasma Gondii in the CNS. J Neuroimmunol. 2010;222:19–28.
63. Mizgerd JP, Lupa MM, Kogan MS, Warren HB, Kobzik L, Topulos GP. Nuclear factor-kappab p50 limits inflammation and prevents lung injury during Escherichia coli pneumonia. Am J Respir Crit Care Med. 2003;168:810–7.
64. Taetzsch T, Benusa S, Levesque S, Mumaw CL, Block ML. Loss of NF-κB p50 function synergistically augments microglial priming in the middle-aged brain. J Neuroinflammation. 2019;16:60.
65. Saldaña M, Mullol J, Aguilar E, Bonastre M, Marin C. Nuclear factor kappa-B p50 and p65 subunits expression in dementia with Lewy bodies. Neuropathol Appl Neurobiol. 2007;33:308–16.
66. Saldaña M, Bonastre M, Aguilar E, Marin C. Role of nigral NFkappaB p50 and p65 subunit expression in haloperidol-induced neurotoxicity and stereotyped behavior in rats. Eur Neuropsychopharmacol. 2006;16:491–7.
67. Karban AS, Okazaki T, Panhuysen CI, Gallegos T, Potter JJ, Bailey-Wilson JE, et al. Functional annotation of a novel NFKB1 promoter polymorphism that increases risk for ulcerative colitis. Hum Mol Genet. 2004;13:35–45.
68. Perez-Oliveira S, Vazquez-Coto D, Pardo S, Blázquez-Estrada M, Menéndez-González M, Siso P et al. NFKB1 variants were associated with the risk of Parkinson´s disease in male. J Neural Transm. 2024.
69. Perkins ND. Integrating cell-signalling pathways with NF-kappaB and IKK function. Nat Rev Mol Cell Biol. 2007;8:49–62.

70. Elsharkawy AM, Oakley F, Lin F, Packham G, Mann DA, Mann J. The NF-kappaB p50:p50:HDAC-1 repressor complex orchestrates transcriptional inhibition of multiple pro-inflammatory genes. J Hepatol. 2010;53:519–27.
71. Bellucci A, Bubacco L, Longhena F, Parrella E, Faustini G, Porrini V, et al. Nuclear Factor-κB dysregulation and α-Synuclein Pathology: critical interplay in the pathogenesis of Parkinson's Disease. Front Aging Neurosci. 2020;12:68.
72. Cao S, Zhang X, Edwards JP, Mosser DM. NF-kappaB1 (p50) homodimers differentially regulate pro- and anti-inflammatory cytokines in macrophages. J Biol Chem. 2006;281:26041–50.
73. Southern SL, Collard TJ, Urban BC, Skeen VR, Smartt HJ, Hague A, et al. BAG-1 interacts with the p50-p50 homodimeric NF-κB complex: implications for colorectal carcinogenesis. Oncogene. 2012;31:2761–72.
74. Sierra A, Abiega O, Shahraz A, Neumann H. Janus-faced microglia: beneficial and detrimental consequences of microglial phagocytosis. Front Cell Neurosci. 2013;7:6.
75. Shannahan JH, Bai W, Brown JM. Implications of scavenger receptors in the safe development of nanotherapeutics. Receptors Clin Investig. 2015;2:e811.
76. Papa S, Rossi F, Ferrari R, Mariani A, De Paola M, Caron I, et al. Selective nanovector mediated treatment of activated proinflammatory microglia/macrophages in spinal cord injury. ACS Nano. 2013;7:9881–95.
77. Frietze S, Farnham PJ. Transcription factor effector domains. Subcell Biochem. 2011;52:261–77.
78. Fani Maleki A, Rivest S. Innate Immune cells: Monocytes, Monocyte-Derived macrophages and Microglia as therapeutic targets for Alzheimer's Disease and multiple sclerosis. Front Cell Neurosci. 2019;13:355.
79. Templeton SP, Kim TS, O'Malley K, Perlman S. Maturation and localization of macrophages and microglia during infection with a neurotropic murine coronavirus. Brain Pathol. 2008;18:40–51.
80. Liu M, Eguchi N, Yamasaki Y, Urade Y, Hattori N, Urabe T. Focal cerebral ischemia/reperfusion injury in mice induces hematopoietic prostaglandin D synthase in microglia and macrophages. Neuroscience. 2007;145:520–9.
81. Kanegawa N, Collste K, Forsberg A, Schain M, Arakawa R, Jucaite A, et al. In vivo evidence of a functional association between immune cells in blood and brain in healthy human subjects. Brain Behav Immun. 2016;54:149–57.
82. Farmen K, Nissen SK, Stokholm MG, Iranzo A, Østergaard K, Serradell M et al. Monocyte markers correlate with immune and neuronal brain changes in REM sleep behavior disorder. Proc Natl Acad Sci U S A. 2021; 118.
83. Cumano A, Godin I. Ontogeny of the hematopoietic system. Annu Rev Immunol. 2007;25:745–85.
84. Meredith GE, Rademacher DJ. MPTP mouse models of Parkinson's disease: an update. J Parkinsons Dis. 2011;1:19–33.
85. Mustapha M, Mat Taib CN. MPTP-induced mouse model of Parkinson's disease: a promising direction of therapeutic strategies. Bosn J Basic Med Sci. 2021;21:422–33.

Publisher's note